Performance and Complexity of Data Acquisition in Compressive-sensing Radar

Christos Tzotzadinis

Master of Science Thesis

TU Delft Delft University of Technology

Electrical Engineering, Mathematics and Computer Science

THALES

Approval MSc Thesis of: .....Christos Tzotzadinis .....

Title: ..... **Performance and Complexity of Data Acquisition in CS Radar**.....

Educational institution: ..... EWI, TU Delft .....

Graduation period:..... 6 March – 8 December, 2017.....

Location/Department:..... *Sensors Advanced Developments Delft* .....

Thales Supervisor:..... *Radmila Pribić* .....

This report (both the paper and electronic version) has been read and commented on by the supervisor of Thales Netherlands B.V. In doing so, the supervisor has reviewed the contents and considering their sensitivity, also information included therein such as floor plans, technical specifications, commercial confidential information and organizational charts that contain names. Based on this, the supervisor has decided the following.

Due to the nature of the assignment/internship results, it was required to create an annex and a modified report for the educational institute. *The annex* and *the rest of the MSc thesis, i.e. the modified report,* are filed under the following categories:

The rest, i.e. the modified report for TU Delft:

☒ This report is **publicly available (Open).** Any defence may take place publicly and the report may be included in public libraries and/or published in knowledge bases.

○ This report and/or a summary thereof is **publicly available to a limited extent (Company Internal).** It will be read and reviewed exclusively by teachers and if necessary by members of the examination board or review committee. The content will be kept confidential and not disseminated through publication or inclusion in public libraries and/or knowledge bases. Digital files are deleted from personal IT resources immediately following graduation, unless the student has obtained explicit permission to keep these files (in part or in full). Any defence of the thesis may take place **in public to a limited extent**. Only relatives to the first degree and teachers of the ...*<name department >*...department may be present at the defence.

The annex:

☒ This report and/or a summary thereof, is **not publicly available (Company Confidential).** It will be reviewed and assessed exclusively by the supervisors within the university/college, possibly by a second reviewer and if necessary by members of the examination board or review committee. The contents shall be kept confidential and not disseminated in any manner whatsoever. The report shall not be published or included in public libraries and/or published in knowledge bases. Digital files shall be deleted from personal IT resources immediately following graduation. Any defence of the thesis must take place **in a closed session** that is, only in the presence of the intern, supervisor(s) and assessors. Where appropriate, an adapted version of report must be prepared for the educational institution.

Approved:	Approved:
Radmila Pribić	*Prof. Geert Leus*
(Thales Supervisor)	(Educational institution)

Delft, 1 December, 2017
(city/date)

THALES

Open

Performance and Complexity of Data Acquisition in Compressive-sensing Radar

MASTER OF SCIENCE THESIS

For the degree of Master of Science in Electrical Engineering at Delft University of Technology

Christos Tzotzadinis

December 7, 2017

DELFT UNIVERSITY OF TECHNOLOGY

DEPARTMENT OF

ELECTRICAL ENGINEERING, MATHEMATICS AND COMPUTER SCIENCE (EWI)

The undersigned hereby certify that they have read and recommend to the Faculty of Electrical Engineering, Mathematics and Computer Science for acceptance a thesis entitled "**Performance and Complexity of Data Acquisition in Compressive-sensing Radar**" by **Christos Tzotzadinis** in partial fulfillment of the requirements for the degree of Master of Science.

Dated: December 7, 2017

Supervisor(s):

prof.dr.ir. Geert Leus, CAS, Delft University of Technology

dr.ir. Radmila Pribić, Sensors Advanced Developments, Thales Nederland

Abstract

Compressive Sensing (CS) provides a new paradigm in data acquisition and signal processing based on the assumption of sparsity and the incoherence of the received signal. Based on that concept, many radar front-end architectures have been studied with the implementation of CS. In these architectures, less data are collected but the radar scene can be recovered through CS with high probability. All these CS front-ends have always been stated as less complicated but never evaluated. The main motivation of this thesis is to find aspects of the complexity and performance which can be used for the characterization of these front-ends like the gain in signal-to-noise ratio (SNR), number of components, power consumption etc. In this thesis, we investigate three radar front-end architectures in CS. The first two are the Multi-Coset (MC) Sampling and Analog-to-Information Converter (AIC) which are widely suggested for telecommunications and radar systems. The third front-end is novel as it contains metamaterial surface antenna elements. The performance and the complexity of each architecture are evaluated. The performance is compared with respect to the conventional reference case of a uniform linear array of antennas.

Acknowledgements

I would like to express my gratitude to all those people who have helped me in these last two years needed to complete my Master of Science.

Firstly, I would like to thank my advisor, Radmila Pribić. A year ago, Mrs. Radmila decided to take a chance on me and give me the opportunity to conduct research as an intern at Thales and then for another period to realize my thesis. Throughout this year, I have learned more than I could possibly imagine while at the same time I gained the best possible start for my career. Mrs. Radmila challenged me to work my hardest and strive for greatness in the field. Also, during the past year working in Thales, I met a lot of really nice colleagues and fellow students who I thank for the pleasant working environment.

My greatest thanks go to my supervisor Geert Leus for his dedication, support, comments, patience and most of all valuable advice on my work. He contributed to my research to a great extent with his presence in our weekly meetings with Mrs. Radmila, providing novel ideas and comments on the project.

Also, I would like to thank my friends for the constant support they have given me throughout my years in Delft and special thanks to my girlfriend Georgia who was with me despite the great distance. She was there in my toughest hours, being patient and supporting giving me courage and keeping me calm.

Of course, nothing of this could happen if it weren't for my family. My special thanks to my sister Anny who helped me with her magnificent skills and her wise advice and of course, my father George and my mother Dimitra who were constantly supporting me in every step I have made so far. I owe them everything I have done so far and my Master of Science is dedicated to them!

Christos Tzotzadinis

Delft, the Netherlands

December 7, 2017

Contents

List of Figures

Notation

$\mathrm{Re}\{\cdot\}$	Real part of complex number
$\mathrm{Im}\{\cdot\}$	Imaginary part of complex number
$\lvert\cdot\rvert$	Absolute value
$\langle\cdot\rangle$	Inner product
$(\cdot)^H$	Hermitian transpose of a vector or a matrix
$\lVert\cdot\rVert_\ell$	ℓ-norm of vector

Symbols

P_T	Transmitted Power
P_R	Received Power
G_A	Gain of antenna
R	Range of target
σ	Radar cross section
A_{eff}	Effective Area of antenna
c	Speed of light
ΔT	Round trip time
f_d	Doppler frequency shift
υ	True velocity of target
k	Boltzmann's constant
T_s	System noise temperature
NF	Noise figure
F	Noise factor
$IP3$	Third-order Intercept Point
$\mathbf{s}$	Unknown signal of interest
$\mathbf{\Psi}$	Orthonormal basis
$\mathbf{\Phi}$	Compression Matrix

$\mathbf{\Theta}$	Sensing Matrix
P_{fa}	Probability of False Alarm
$\mathbf{y}$	Measurement vector
$\mathbf{n}$	Additive Noise
θ	Angle of arrival
$\mu(\mathbf{\Theta})$	Mutual coherence of matrix Θ
h	Threshold of SSP
M	Number of antenna elements
L	Number of metamaterial surfaces
C	Number of equivalent antenna elements
B	Bandwidth
P	Reduced number of antenna elements
$u_{rc}(t)$	Continuous received time signal
t	Time index
x_m	Position of m-th antenna element
$s(t)$	Complex baseband signal
fc	Carrier frequency
f_{IF}	Intermediate frequency
λ	Wavelength
Δ	Distance between two antenna elements
τ	Time delay
D	Aperture of the radar system
d	Size of antenna element
P_{out}^{ULA}	Signal power at the output of the ULA
N_{out}^{ULA}	Noise power at the output of the ULA
$\mathbf{a}(\theta)$	Array vector response
γ	Noise variance
$\mathbf{y}_{MC}$	Output vector of MC
$\mathbf{H}_{MC}$	Selection matrix of MC
c_p	MC pattern
$\mathbf{H}_{AIC}$	Compression matrix of AIC

ϕ	Phase shift
$\mathbf{H}_{MS}$	Compression matrix of MS
$\mathbf{y}_{MS}$	Output vector of MS
g_{mss}	Gain of metamaterial surface

Abbreviations

CS	Compressive Sensing
ADC	Analog to Digital Converter
RF	Radio Frequency
SNR	Signal to Noise Ratio
SSP	Sparse Signal Processing
DSP	Digital Signal Processing
Radar	Radio Detection And Ranging
EM	Electromagnetic
PRI	Pulse Repetition Interval
PRF	Pulse Repetition Frequency
RCS	Radar Cross Section
PD	Pulse Doppler
CW	Constant Wave
CVR	Crystal Video Receiver
BPF	Bandpass Filter
LPF	Lowpass Filter
IF	Intermediate Frequency
LNA	Low Noise Amplifier
LO	Local Oscillator
DC	Direct Current
PSD	Power Spectral Density
RIP	Restricted Isometry Property
ULA	Uniformm Linear Array of Antennas

AIC	Analog to Information Converter
MC	Multi-coset
MF	Matched Filtering
MS	Metamaterial Surface
MWC	Modulated Wideband Converter
SAR	Synthetic Aperture Radar
cELC	complementary Electric Inductive Capacitors
PCB	Printed Circuit Board
LFM	Linearly Frequency Modulated
ULMA	Uniform Linear Array of Metamaterial-surface antennas
AGC	Automatic Gain Control
DOA	Directions of Arrival
SSR	Sparse Signal Recovery

Chapter 1

Introduction

The aim of this thesis is to evaluate the performance and complexity of compressive-sensing (CS) systems with respect to different designs of data acquisition in the front end with examples from radar (but not limited to radar). This chapter provides the motivation for introducing alternative data acquisition schemes to CS systems and the main contribution of the thesis.

1-1 Motivation

The gradual progress in modern electronics, constantly gives rise to new ways in radar systems and their data-acquisition front ends. The manufacturing of new analogue-to-digital converters (ADC) which are capable of sampling at GHz, makes it possible to sample the radio frequency (RF) signal directly but this cannot happen without the use of a digitally programmable system. Traditionally, the radar receiver designs consist of mixing stages which alter the carrier frequencys of the received signal in order to be sampled at a low rate. These stages include additional operations like filtering, amplification and others, which increase the complexity of the radar receiver and thereafter, the cost, the development and the manufacturing of the whole system.

The radar system is similar to a communication system as shown in Figure 1-1. In a system like this, the information is transmitted by the transmitter, it travels through the transmission medium and then it arrives at the receiver which captures the signal, processes and sends information to the

user. In a similar way, in a radar system, the transmitter sends a signal to the field of view where a target exists and then, the transmitted signal hits the target and reflects back. So, the receiver which is located in the same place as the transmitter, captures the reflected signal. The first part in a radar receiver is its front end. Its role is very important since it acquires the data which will be used to extract the information. So, it is crucial that the data acquisition system is both accurate and beneficial.

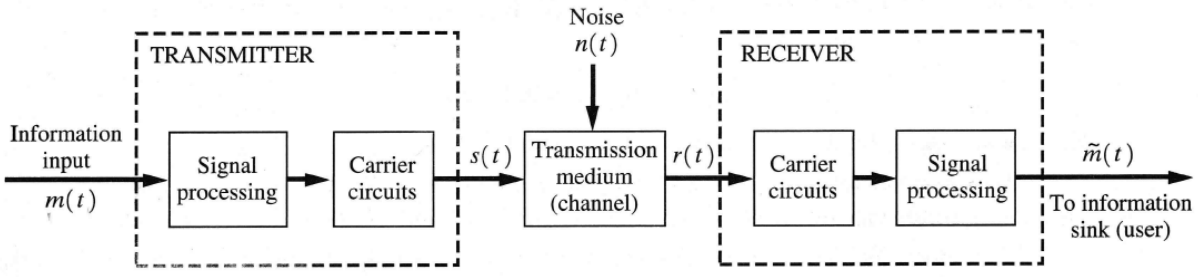

Figure 1-1: Generic Communication System.

Many researchers have been involved in the design and implementation of radar receivers. After years of research, the technology has reached a level where the accurate data acquisition in radar systems is not enough. The most recent radar front ends are making use of compressive techniques in the signal reception which acquire less data. The CS (radar) front ends have been studied for many years to make them less complicated, but never this has been evaluated. In general, the CS front-end architectures have been assumed for many years to be less complicated although the complexity had never been evaluated. This work fills the gap by trying to establish the balance between the performance and the complexity of typical CS front ends.

1-2 Research Goals

The purpose of this project is to analyze the performance and the complexity of different front-end architectures in compressive sensing. In addition, a novel scheme is proposed which may be more beneficial than the traditional CS front ends.

At first, a full analysis of the traditional front ends in RF receivers which are used in radar systems will be presented. Furthermore, a model of a conventional radar front end will be used as a reference case. The other CS front ends will be evaluated with respect to the reference case. The

intention is to find the best balance between the complexity of the components in the front end of radar systems and the front-end performance which shall be comparable with (or even better than) the reference case. The front-end complexity consists of a number of essential components which would be needed. The front-end performance is measured with respect to the signal-to-noise ratio (SNR) that it would produce at its output with a known input. Finally, the performance of the different front-end architectures will be illustrated with results from the CS radar back end containing sparse signal processing (SSP).

The goals of this thesis project can be briefly summarized as follows:

- Presentation of CS, data acquisition architectures in CS radar systems, radar measurements and their processing,
- Investigating complexity/costs of two state-of-the-art designs of CS data acquisition,
- Proposing a novel CS data acquisition design which involves metamaterial surfaces,
- Implementing the performance analysis for particular spatial measurements in MATLAB,
- Evaluating the performance-complexity balance of the designs.

1-3 Contributions

This work provides a complete framework for a radar system's front end and its application in CS. Starting from signal reception by the radar system, we model the total operation of the data acquisition system taking into account all the essential components of a modern radar receiver.

We demonstrate how CS radar can reduce the sampling rate in space or equivalently, how it can reduce the number of antenna elements. Accordingly, the cost of the architecture, the needed memory and the size of the radar receiver seem to be reduced. On the other hand, these benefits come with the drawback of high complexity since more components are needed for the implementation of the CS and so, additional adjustments between them, as well. We have considered two state-of-the-art CS radar architectures, the Multi-Coset (MC) sampling and the Analog-to-Information Converter (AIC). We present their model, their benefits and their drawbacks. In addition, we propose a novel radar front-end scheme which contains metamaterial surface antenna elements. This architecture

promises comparable performance with the other two but with low complexity since less components are used. Lastly, these three CS radar systems are presented with respect to the reference case of a uniform linear array of antennas (ULA).

1-4 Thesis Outline

The master thesis report is organized as follows:

- Chapter 2 introduces the basic theory and principles of radar systems for the readers who are unfamiliar with that field. Starting from the way a radar system transmits and receives a signal, we give some further insight in the RF receivers which are mainly digital nowadays and present the necessary steps for the calculation of the important parameters which characterize the RF receivers.
- In Chapter 3 we review the CS framework and introduce the main criteria related to the quality of the sensing matrix. In addition, we go one step further by presenting the CS radar system and the major concepts for its implementation.
- Chapter 4 describes analytically each data acquisition scheme. It starts with a reference case which is mainly used in traditional radar receivers, followed by two state-of-the-art architectures in CS. Lastly, a novel scheme is presented which promises comparable performance with the previous architectures and smaller size.
- Chapter 5 lays out our main results from the balance between the complexity and the performance of the four data acquisition schemes described in Chapter 4.
- Chapter 6 summarizes our findings and points out our conclusions, recommendations and suggestions for future work.

Chapter 2

Basic Principles of Modern Radar Systems

This chapter starts with an introduction of the radar concept, presents the basic radar functionality with emphasis on obtaining the information about a target. Furthermore, we present existing radar receivers and select the front end which will be used in the next chapters. Lastly, we show how the important parameters of a receiver front end are calculated for the determination of its sensitivity.

2-1 Introduction and Overview

Radar (Radio Detection and Ranging) is an RF system which is used to locate an object such as airplanes, ships, vehicles, weather incidents like precipitations, or even the natural environment. This is done by transmitting a known signal towards the field of its view and then detecting the echo signal reflected from the object which may be present in the surrounding space. This reflected energy can show not only if a target is present or not, but also when the target is present, it can give information about its location, its velocity, its shape and other target information.

As we have already mentioned, the operation starts with the transmission of an electromagnetic (EM) wave of a certain frequency which depends on the application. This EM wave travels through a medium and a portion of it hits a target and travels back to the radar receiver where a portion of the backscattered field is captured by its antenna, as shown in Figure 2-1. At this point, we can distinguish two different types of radar systems depending on the type of transmission and receive

configurations: monostatic and bistatic. In a monostatic configuration, the co-located antenna is used for both transmission and reception of the signal whereas, in a bistatic configuration there are two different antennas for transmission and reception at different positions.

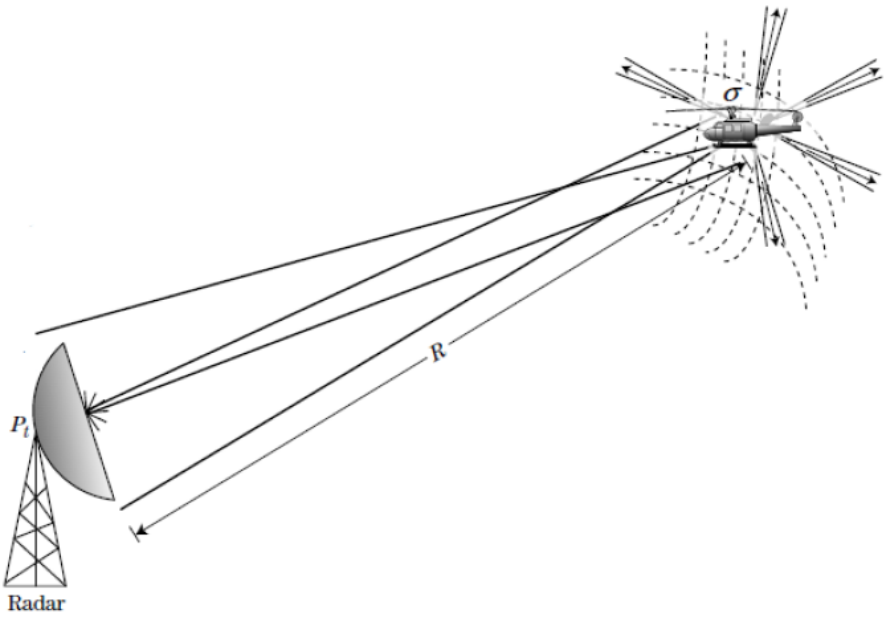

Figure 2-1: Traditional radar system.

In practice, most of the radar systems radiate the power P_T towards a specific direction so the respective antenna has a gain G_A. So, if a target reflects back all the power intercepted by its effective area σ isotropically, then this reflected power density is given by the equation:

$$P_{ref} = \frac{P_T \cdot G_A \cdot \sigma}{(4\pi R^2)^2} \tag{2-1}$$

where R is the range of the target. Lastly, if A_{eff} is the effective area of the receiving antenna, the received power by that antenna will be:

$$P_R = P_{ref} \cdot A_{eff} = \frac{P_T \cdot G_A \cdot A_{eff} \cdot \sigma}{(4\pi R^2)^2} \tag{2-2}$$

This radar equation is developed assuming that the target has an effective area σ and an isotropic reflection pattern. In general, most of the targets are not isotropic and have different effective areas. So, in order to be more accurate,we call σ the radar cross section (RCS), which represents the area of an isotropic target which would reflect the same return power as the real target.

Another way to characterize the radar system is with respect to the transmitted signal. There are two main categories: the pulsed-Doppler (PD) and the continuous wave (CW) radars. In order to

proceed to the main functionality of a radar system we will focus only on a PD radar. For an interested reader, a lot of information related to CW radar systems can be found in the literature [1].

2-1-1 Range Estimation

In a radar system, the signal waveform is crucial for the accuracy, resolution and ambiguity in determining the range and the velocity (range rate) of a target. In the PD radar case, monostatic configuration is mainly used. The radar system transmits EM waves during a short time interval, i.e. pulse width τ. In this time interval, the antenna is isolated from the receiver. After the transmission of the first pulse, there is a "listening" time interval where the receiver is expecting to receive the echo from the target. So, pulses are transmitted at a rate of $PRF = \frac{1}{PRI}$, where PRF is the pulse repetition frequency and PRI is the pulse repetition interval or the "listening" time interval together with the pulse width τ. Figure 2-2 [1] illustrates the operation of a pulse Doppler radar system. If ΔT is the

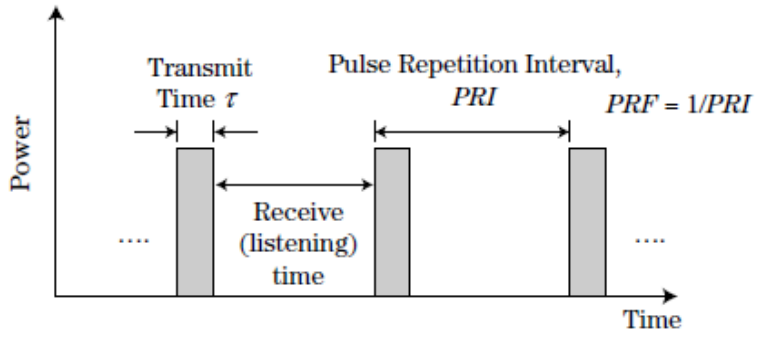

Figure 2-2: Pulse Radar Waveform.

round trip delay between the transmitted signal and the reflected echo, then the range of the target can be calculated as follows

$$R = \frac{1}{2} \cdot c \cdot \Delta T, \tag{2-3}$$

where c is the speed of light in free space. Lastly, if the reflected pulse of the fist transmitted pulse arrives to the receiver during the first "listening" time interval, then the range can be estimated unambiguously. On the other hand, if it arrives during any next "listening" time interval, then the range is ambiguous because of the uncertainty of which transmitted pulse caused the reflected one. Thus, the maximum unambiguous range is defined as:

$$R_{unamb_{max}} = \frac{1}{2} \cdot c \cdot PRI \tag{2-4}$$

2-1-2 Velocity Estimation

Radar systems can also sense the motion of the target, by exploiting the fact that a moving target has a radial velocity υ_d, causing the frequency of the reflected signal to be different. This is called the Doppler effect, common to all wave phenomena. The Doppler effect states that when a target is moving, the received signal will have a frequency equal to the initial carrier plus a Doppler shift which will depend on the direction and the speed of the target. In other words, if the target is moving towards the radar systems, the Doppler shift will be positive and the frequency of the echo will be larger than the initial one. On the other hand, if the target is moving away, the Doppler shift will be negative and the signal's frequency will be smaller than the initial one [2]. The relation between the Doppler shift f_d and the velocity υ of the target, is given by:

$$f_d = \frac{2 \cdot \upsilon}{\lambda} \cdot cos(\phi) = \frac{2 \cdot \upsilon_d}{\lambda} \tag{2-5}$$

where $\lambda = \frac{c}{fc}$ is the wavelength of the signal, f_c is the carrier frequency and ϕ is the angle between the actual target velocity υ and the straight line which connects the target and the radar receiver. Lastly, we must point that as PD is ambiguous in range, it can also be ambiguous in Doppler. That is because most modern PD radars sample the Doppler frequency shift at the PRF due to the Nyquist theorem. This leads to Doppler frequency ambiguity if the sampling rate is not sufficient. As a result, the maximum Doppler shift frequency that can be unambiguously estimated is:

$$f_{d_{max}} = \pm \frac{PRF}{2} \tag{2-6}$$

In a similar way, the maximum unambiguous radial velocity that can be estimated will be:

$$\upsilon_{d_{max}} = \pm \frac{PRF \cdot \lambda}{4} \tag{2-7}$$

2-1-3 Angle of Arrival Estimation

Modern radar systems can also determine an angular position of a target. This angular position is described by the elevation and azimuth angles. It is determined by the pointing angle of the antenna's main beam during the sensing procedure [1]. Phased arrays are the most used type in radar systems because they provide high reliability, and good sidelobe control. They are applicable in both beam steering at transmission and estimation of angle of arrival at the reception.

In order to explain the procedure of estimating the direction of arrival (DOA), we need the standard mathematical model of the received radar signal from different sources. The received signal y_m at time instance t from K point sources at the m-th element of an array of antennas can be written as:

$$y_m(t) = \sum_{k=1}^{K} a_k \cdot \mathbf{s}_k(\theta_k, f_{d_k}, r_k) = \sum_{k=1}^{K} a_k \cdot u(t - \Delta T_k - \tau_m(t)) e^{-j2\pi f_{d_k} t} e^{j2\pi f_c (t - \Delta T_k - \tau_m(t))} \tag{2-8}$$

where a_k is the amplitude of the k-th point source, $u(t)$ is the transmitted signal, ΔT_k is the corresponding round trip delay of the signal, f_{d_k} is the Doppler frequency shift and f_c is the carrier frequency and finally, $\tau_m(t)$ is the time delay of the signal between the m-th antenna element and the first element of the array. This time delay depends on the position of the m-th antenna element and is related to the DOA θ_k of the k-th target as $\tau_m(t) = -\frac{x_m(t) sin(\theta_k)}{c}$ where x_m is the position of the element in the antenna array. The DOA θ can be either a single angle or a vector of the two angles azimuth and elevation angles. In angle estimation, the DOA is expressed as a function of the delay of the signal between two antenna elements. As a result, by computing this delay, we can estimate the DOA.

The most common way to estimate the angle DOA is by beamforming. The objective of beamforming is to iteratively apply a receiver weight vector $\mathbf{w}_k$, which usually takes the form of phase shifts, such that the estimated output is:

$$\hat{\mathbf{s}}_k(\theta_k, f_{d_k}, r_k) = \mathbf{w}_k^H y_m \tag{2-9}$$

and search for the maximum. In other words, we want the output of the weight vector $\mathbf{w}_k$ to be an estimate of the k-th source. Which beamformer is the "best" depends on the optimality criterion, of which there are many. We will see the DOA estimation in more details in Chapter 4.

2-2 Radar Receivers

In a radar system, the role of the receiver front end is to capture the signal and convert it to an appropriate form for processing. When the signal arrives at the antenna, it is very weak and has a high frequency. As a result, radar receivers are used to amplify, down-convert the RF signal to the baseband with minimal added distortion and in the end, digitize the analog baseband signal. The choice of the receiver architecture is related to the complexity, power dissipation and system consideration. The RF receiver architecture can be classified with respect to the down conversion.

2-2-1 Crystal Video Receiver

The crystal video receiver (CVR), is the simplest type of receiver configuration where the input signal is coupled to a detector to convert the RF signal directly to video. Then the video output is amplified before providing the signal to the processor [1].

As it is shown if Figure 2-3, a crystal receiver consists of a bandpass filter (BPF) which filters the out of band frequencies, a crystal detector and a video amplifier. The main disadvantage of this architecture is its sensitivity which is very low because of the low rectification efficiency of the detecting elements at small signal levels. In addition, all the amplifications are done by the video amplifier so the received pulses are normally distorted [1]. Due to these drawbacks, the CVR is mainly used in short range systems like automotive collision avoidance.

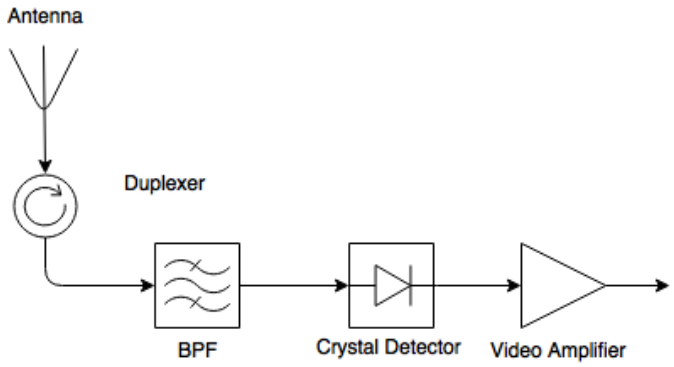

Figure 2-3: Crystal Video Receiver.

An improved version of the CVR is shown in Figure 2-4 where an RF amplifier is placed before the detection for the improvement of the sensitivity of the receiver and the increase of the SNR at the output of the detection. The disadvantage of this adding comes with additional costs like power consumption, complexity and size.

2-2-2 Homodyne Receiver

The homodyne or direct down-conversion receiver is a configuration which moves the RF signal directly to the baseband [3]. This is done by mixing the received RF signal with the carrier frequency f_c of the transmitter. It is obvious that we are talking about a very simple scheme since there are no

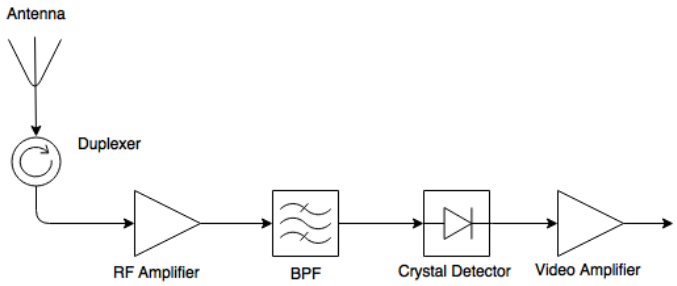

Figure 2-4: Modified Crystal Video Receiver.

intermediate frequency (IF) down conversions and thus, less components are used at it is shown in Figure 2-5.

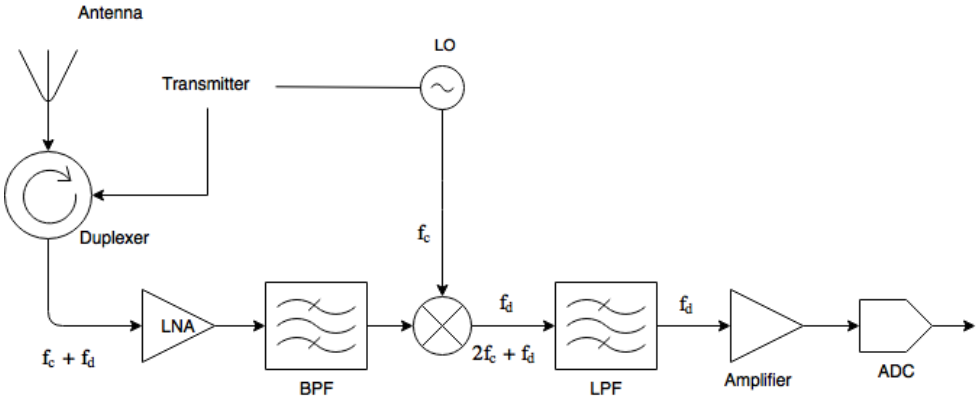

Figure 2-5: Homodyne Receiver.

A homodyne receiver consists of a circulator which is a ferromagnetic device coupling the transmitting signal to the antenna while isolating it from the receiver, a low noise amplifier (LNA), a BPF which filters the out-of-band frequencies, a local oscillator (LO) which is tuned to the desired RF signal, a mixer which mixes the received RF carrier with the frequency of the LO, a low pass filter (LPF) which filters out the right side band after the mixing, an amplifier and an ADC which samples the signal at Nyquist rate.

The main disadvantage of this radar receiver is present during the implementation in CMOS technology where very high noise figures occur due to the implementation of active mixers. Also, parasitic direct current (DC) signals appear due to mismatch, self reception and RF crosstalk [4]. Lastly, the LO of the homodyne receiver is tuned to RF frequencies for transmission so there is a possibility the receiver LO may interfere with other nearby receivers tuned to the same frequencies.

Still, it has been seen that the sensitivity is considerably improved compared to the CVR [1].

2-2-3 Heterodyne Receiver

The heterodyne receiver, shown in Figure 2-6, was first introduced as an RF receiver containing an LO for down conversion of the signal to a common IF frequency. The superheterodyne receiver is essentially the same thing except that the LO is tunable. This advantage is more obvious in the case where the radar systems are using frequency diversity or specialized processing waveforms, so the LO frequency tuning is compulsory.

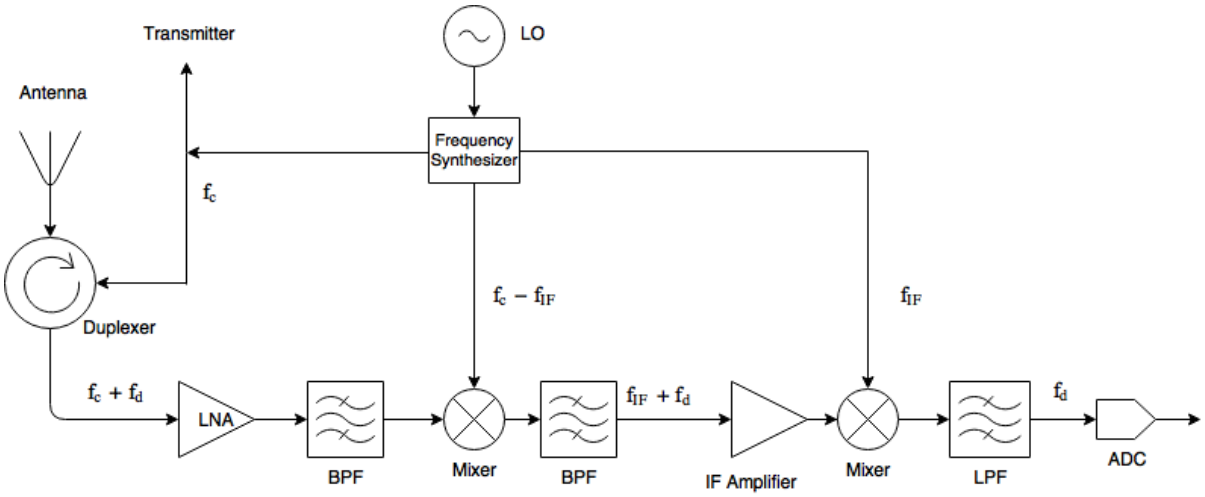

Figure 2-6: Supereterodyne Receiver.

As shown in Figure 2-6, the received signal from the antenna is coupled through the circulator to the mixer. In many current applications, immediately after the circulator, an LNA increases the amplitude of the weak signal. Then, a BPF follows which is a wideband low-loss, pre-select filter which provides out of band frequency rejection and prevents signals that are far from the actual pass band to saturate the operation. After the basic components which are mainly used in every kind of receiver, it comes the part of the receiver which performs its actual function. Here, there are two stages of down-conversion of the signal to the baseband. The first one, as we already said, downconverts the input RF signal to an IF and then, the IF signal is amplified and filtered by a BPF for the rejection of the unwanted mixer products and out of band signals. A second similar stage is following for moving the IF signal to baseband before the digitization by the ADC.

The main advantage of the superheterodyne receiver is that it contains a zero IF receiver so

it attains better immunity from interfering signals and better sensitivity. On the other hand since there are more components the cost and the size of the receiver will be larger. So, for the rest of the thesis, the superheterodyne receiver will be the RF receiver since it is the state-of-the-art in higher sensitivity and better performance.

2-3 Radar Receiver Sensitivity

In a radar system, the backscattered field from a target is always weak and it exists in the presence of interference. The interference comes in four different ways [1]: a) internal and external electronic noise, b) reflected EM waves from objects in the environment c) unintentional EM waves from human hand - made sources and d) intentional jamming from electronic counter measures. The internal electronic noise is caused by EM waves, which occurs always at all frequencies is called thermal noise. The thermal noise is generated because of the thermal perturbation of the electrons which are moving within an electric conductor. Essentially, the thermal noise is produced by every object with temperature above absolute zero regardless of the applied voltage, so it depends on the temperature of the respective component. The radar receiver contains electronic device like amplifiers, filters, mixers etc. which produce own thermal noise. As a result, we would prefer the signal level to be greater than the noise level and the interference level so that the radar receiver can capture more information about the target from the signal.

At the very beginning of the radar reception, an antenna collects the backscattered field. This antenna element can be a waveguide, a probe antenna, a horn antenna or even a surface made of a specific material. After the reception by the antenna element, the signal passes through a feed line and is driven to the next receiver stage which is an LNA. This LNA preamplifies the signal and introduces only a small amount of thermal noise. Since the analog components of the receiver introduce thermal noise, the challenge is design a front end that introduces the least amount of noise into the signal of a radar receiver.

The thermal noise is uniformly distributed and its power spectral density (PSD) is constant in all the frequencies. Despite this fact, the radar receiver captures noise only in the frequencies in which the radar system is susceptible. These frequencies are determined by the radar's bandwidth B.

So, the power N of the thermal noise is given by:

$$N = k \cdot T_s \cdot B = k \cdot T_0 \cdot F \cdot B \tag{2-10}$$

where

k is Boltzmann's constant (1.38 x 10^{-23} watt-sec/K)

T_0 is the standard temperature (290 K)

T_s is the system noise temperature ($T_s = T_0 \cdot F$)

B is the instantaneous receiver bandwidth in Hz

F is the noise factor of the receiver subsystem (unitless).

Observing equation (2-10) we can see that the noise power of the receiver is linear proportional to its bandwidth but the problem is that we can't make it small in order to reduce the noise power without affecting the target signal and the radar performance. In addition, the noise figure, $NF = 10log_{10}(F)$, is an alternate method to describe the receiver noise at a system temperature T_s. Thus, we can calculate the receiver noise power by calculating the overall noise figure.

In an RF receiver, the analog components which introduce noise are amplifiers, filters, mixers, LO etc. After many years of development, a wide area of different components is available since they are designed with different frequency ranges, noise figures and gains depending on the type of the analog or digital receiver. As a result, when we want to optimally match the components of a receiver with analog-to-digital converter, we can choose a specific combination of different amplifiers to be connected, since they can be treated as a single one for the calculation of their performance [5]. By saying "optimally", the desired sensitivity and dynamic range are meant.

On the other hand, the technology of ADCs at high sampling frequencies with a high number of bits is at the stage of infancy and also, this kind of ADCs requires a large amount of energy. Thus, because of the limited available high speed ADCs, when we design an RF receiver, we first select the ADC and then the components for which the performance meets the demands of the respective ADC [5].

At first, let us define the basic parameters of a receiver's stage which are the gain (G), the noise figure (NF) and the third-order intercept point ($IP3$). The gain of a component is defined as the

ratio of the output signal power of the component to the input signal power which can be written as

$$G = \frac{P_{out}}{P_{in}} \tag{2-11}$$

The noise factor is defined as the ratio of the output noise power of a device to the power attributable to thermal noise in the input termination at standard noise temperature T_0 (usually 290K). In a similar way, the noise figure is simply the noise factor expressed in dB and describes the degradation of the SNR of a signal through its pass from the component. Lastly, the IP3 is a parameter which has to do with the linearity of a component. When an amplifier, for instance, becomes non-linear, it produces harmonics of the amplified input. The second, third, and higher harmonics are usually out of the receiver's bandwidth, so they are all easily filtered out by the receiver's filters. However, non-linearity will also produce a mixing effect of two or more signals. For example, if two signals are close together in frequency, some of the sum and difference frequencies can occur within the bandwidth of the amplifier. These cannot be filtered out, so they will ultimately become interfering signals to the main received signals [5].

The gains of the components are usually given by the manufacturer. In the simplest case where we have multiple amplifiers connected in cascade, we take into account these important parameters and calculate the overall performance of the chain. In general, we want the chain to have the lowest possible noise figure. For n cascaded amplifiers in a chain, the overall gain will be

$$G = G_1 \cdot G_2 \ldots G_n. \tag{2-12}$$

The overall noise factor of the amplifiers connected in cascade will be

$$F = F_1 + \frac{F_2 - 1}{G,} + \frac{F_3 - 1}{G_1 G_2} + \cdots + \frac{F_n - 1}{G_1 G_2 \ldots G_n}, \tag{2-13}$$

where F_i is the noise factor of the i-th amplifier [5]. Observing this equation, one can point that when the gain G_i is very large, then the overall noise figure is determined by $F_1, F_2, \cdots, F_{i-1}$. In other words, the overall noise figure of a receiver is highly dependent on the first component with high gain and all the components before that. Usually, the first component with high gain is an amplifier. Thus, all the components after that will have a minor effect on the overall noise figure. In general, RF amplifiers have high gain and can be briefly divided into two categories: the ones with low noise and the ones with high power. The LNAs usually have low IP3 whereas, the high power amplifiers have a high noise figure. As a result, if we take into account what we mentioned before concerning the role of the

first high gain component, it is wise to put the LNAs at the beginning of the receiver's chain and the high power amplifiers at the end of the chain. In plain words, we can say that the noise is dominated by the first amplifier.

If the respective receiver's component is active, like an amplifier, then its gain and noise figure is given in the data sheet of the manufacturer. On the other hand, when the component is passive (attenuator or filter) then the important parameters are not given except the insertion losses. In that case, the gain will be the negative value of the insertion losses and the noise figure equals the insertion losses. The IP3 is partially given by the manufacturer but we can briefly describe the way we can calculate it. The intercept point is obtained graphically by plotting the output power versus the input power both on logarithmic scales (e.g., decibels). In the graph, there are two curves: the one for linearly amplified signal at an input tone frequency and the one for a nonlinear product. On a logarithmic scale, the n-th order function will be a straight line with a slope of n. Therefore, the linearly amplified signal will exhibit a slope of 1. A third-order nonlinear product will increase by 3 dB in power when the input power is raised by 1 dB. So, the point will be the one where the curves intersect. An example is given in Figure 2-7. We can also use:

$$IIP_3(dBm) = P_{in}(dBm) - IMD_3(dBc)/2 \tag{2-14}$$

where IMD_3 is the third order intermodulation distortion which is given by the manufacturer.

For the case of an ADC, the important parameters are given by the manufacturer in the data sheet. The most important of them are the resolution bits, which are used for each quantization level, the sampling rate, the SNR and the maximum input power which can be employed without saturating the device. Since we know these data, we can calculate the noise figure of the ADC. The procedure for calculating its noise figure starts with the calculation of the full-scale input power. Since the peak-to-peak voltage V_{pp} and the input impedance Z_{in} are given by the manufacturer, then the full-scale power is given by:

$$P_{Fullscale}[dBm] = 10log_{10}(1000 \cdot \frac{V_{rms}^2}{Z_{in}}) \tag{2-15}$$

where $V_{rms} = \frac{V_{pp}/2}{\sqrt{2}}$. The next step in the NF calculation is to calculate the effective input noise of the ADC from its SNR. The SNR of the ADC is shown on the data sheet for a variety of input frequencies. We just have to use the value corresponding to the IF input frequency of interest. Therefore, we can calculate the noise figure in dB using equation (2-10) as follows:

$$NF_{ADC} = P_{Fullscale}[dBm] - 10log_{10}(kT) - SNR_{ADC} - 10log_{10}(B) \tag{2-16}$$

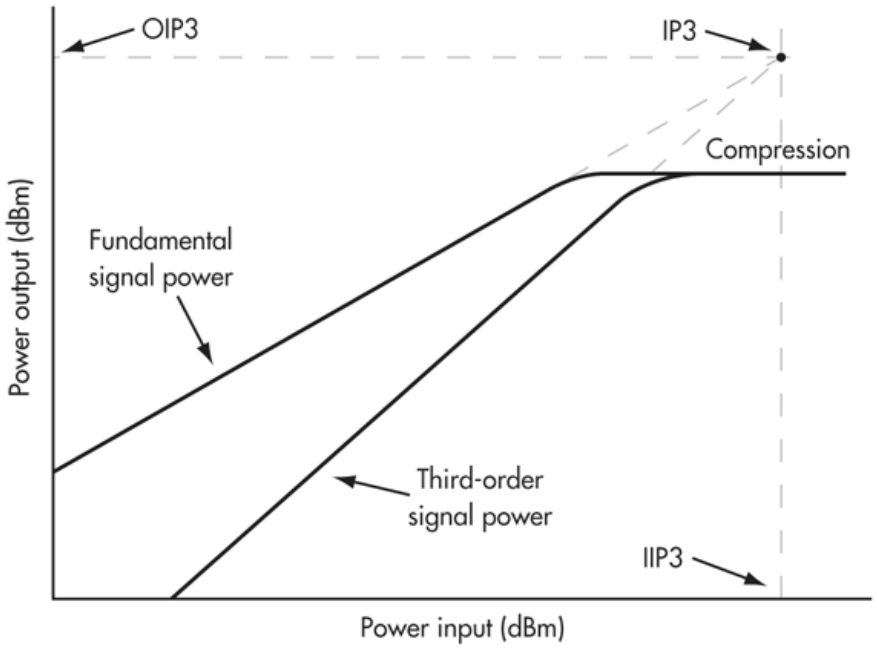

Figure 2-7: Third-order intercept point

2-4 Conclusions

This chapter expands the basic concept that we meet in modern radar systems which are used in the next chapters. We explain the way radar performs, the techniques for range, velocity and angle estimation, and we also present a few radar receivers which are widely used. Lastly, we present the way we can calculate the sensitivity and the important parameters of the superheterodyne receiver and the components that are chosen.

Chapter 3

Compressive Sensing

In this chapter we will present the paradigm of CS and the way it can be applied in radar systems. We will analyze the concept of sparsity and incoherence, the importance of choosing the right sensing matrix and lastly, the SSP framework.

3-1 Introduction to Compressive Sensing

As it has been seen is Chapter 2, the last part in an RF receiver is the ADC which samples the analog signal and moves it to the digital domain. Conventional approaches to sampling a signal or an image, use the Shannon-Nyquist theorem [6]. This theorem states that if a real-valued signal has a bandwidth B then it is completely specified by sampling it at rate at least twice the maximum frequency presented in the signal i.e. $f_s = 2B$. For that reason, all the ADCs used in the architectures of Chapter 2, are uniformly sampling the analog RF signal at or above the Nyquist rate.

The gradual evolution of technology has shown that most of the times, the information we get by sampling a signal at Nyquist rate, is redundant and most of the data are thrown away afterwards since only a small portion of them are useful for the complete information acquisition. This fact gave rise to CS theory introduced by Candès [7], Romberg and Tao [8] and Donoho [9], which asserts that one can recover certain signals and images from far fewer samples or measurements than the traditional methods [7]. For this to hold, CS relies on two principles: sparsity and incoherence.

- Sparsity means that the information density of a continuous time signal may be much smaller than its bandwidth. More specifically, when a signal is sparse or compressible it can be represented with only a few coefficients compared to its dimensionality, when expressed in a proper basis.

- Incoherence means that the sensing and representation matrices must be as weakly correlated as possible. This ensures that the information is not damaged by the sensing.

3-2 Sparsity

Let us say that we have a signal vector $\mathbf{s} \in \mathbb{C}^N$ which is expanded in an orthonormal basis $\mathbf{\Psi} = [\boldsymbol{\psi}_1, \boldsymbol{\psi}_2, ..., \boldsymbol{\psi}_N]$ as follows:

$$\mathbf{s} = \mathbf{\Psi X} \tag{3-1}$$

where $\mathbf{x} \in \mathbb{C}^N$ is the coefficient sequence. By saying that the signal $\mathbf{x}$ is K-sparse, we mean that only $K \ll N$ of the coefficients are non zero. So, the signal $\mathbf{x}$ which is K-sparse can be recovered from less non adaptive linear projections onto a second basis $\mathbf{\Phi}$ which will be incoherent with the first one. More specifically, compression means to find an orthogonal MxN compression matrix $\mathbf{\Phi}$ with $M < N$, which by applying it to the signal $\mathbf{x}$ will yield:

$$\mathbf{y} = \mathbf{\Phi} \cdot \mathbf{s} = \mathbf{\Phi} \cdot \mathbf{\Psi} \cdot \mathbf{x} = \mathbf{\Theta} \cdot \mathbf{x} \tag{3-2}$$

where $\mathbf{\Theta} \in \mathbb{C}^{MxN}$ is the sensing matrix and $\mathbf{y} \in \mathbb{C}^N$ is the measurement vector. In plain words, one can throw away a fraction of the coefficients and reconstruct the signal with high probability.

3-3 Incoherence

As we said previously, CS starts with a pair of matrices. The first basis $\mathbf{\Phi}$ is the compression matrix which depends on the type of CS system and the matrix $\mathbf{\Psi}$ which is the signal representation matrix. This pair formulates the sensing matrix $\mathbf{\Theta}$ whose columns are to be as much linearly independent as possible. There are three ways to measure the incoherence in matrix $\mathbf{\Theta}$: the restricted isometry property (RIP), the null-space property and the mutual coherence. In the following sections, the RIP and the mutual coherence are explained.

3-3-1 Restricted Isometry Property

The RIP states that for a signal $\mathbf{s} = \mathbf{\Psi x}$, the sensing matrix $\mathbf{\Theta}$ with normalized columns satisfies the RIP (k, δ_k) of order k and an isometry constant δ_k if:

$$(1-\delta_k)\|\mathbf{x}\|_2^2 \leq \|\mathbf{\Theta x}\|_2^2 \leq (1+\delta_k)\|\mathbf{x}\|_2^2 \tag{3-3}$$

for every k-sparse vector $\mathbf{x} \in \mathbb{C}^{Nx1}$. When RIP holds, $\mathbf{\Theta}$ approximately preserves the Euclidean length of K-sparse signals [7]. Equivalently, we can say that all subsets of K columns taken from Θ are nearly orthogonal. The RIP also guarantees stability of the CS problem solution under noise [8].

3-3-2 Mutual Coherence

The mutual coherence $\mu(\mathbf{\Theta})$ is the most common choice for the evolution of the incoherence of matrix $\mathbf{\Theta}$ because it is easy to be computed. It is expressed as:

$$\mu(\mathbf{\Theta}) = \max_{i \neq t} |\langle \theta_i, \theta_t \rangle| \tag{3-4}$$

where θ_n is the n-th normalized column, $n = 1, 2, \cdots N$ of the matrix $\mathbf{\Theta}$ and the operation $\langle \cdot \rangle$ is the inner product. Alternatively, since $\mathbf{\Theta} = \mathbf{\Phi} \cdot \mathbf{\Psi}$, we can say that mutual coherence measures the largest correlation between any two columns of $\mathbf{\Phi}$ and $\mathbf{\Psi}$ [7]. From linear algebra, it holds that $\mu(\mathbf{\Theta}) \in [0, 1]$ so, if the mutual coherence is zero, then the columns of $\mathbf{\Theta}$ are orthogonal. The mutual coherence can also be viewed as the maximum of the off-diagonal elements of matrix $\mathbf{\Theta}^H\mathbf{\Theta}$, where $(\cdot)^H$ is the Hermitian matrix [10].

The importance of the mutual coherence is obvious in reconstruction algorithms and also contributes to the lower bound on the number of measurements M that are needed for the reconstruction [11] since:

$$M \geq C \cdot \mu^2(\mathbf{\Theta}) \cdot K \cdot logN \tag{3-5}$$

for some positive constant C and a random $\mathbf{\Theta}$. So, it is obvious that the smaller the coherence, the fewer samples are needed.

3-4 Sparse Signal Processing

In the back end of a CS radar system, the SSP is a major part in radar processing from fewer measurements, as already explained in this chapter.

At first, we must say that we can use basic linear algebra to solve problem 3-2 but since it is underdetermined, it has infinite number of solutions. That is why we take advantage of a-priori knowledge of the signal $\mathbf{x}$ being its sparsity. So, if we search for the sparsest $\mathbf{x}$, we can find a unique solution to the problem.

As we know from literature [9], the ℓ_0 norm $\| \mathbf{x} \|_0$ is the number of non zeros in $\mathbf{x}$ so, we can define the solution $\mathbf{x}$ as:

$$\begin{aligned} \hat{\mathbf{x}} &= arg\min_x \|\mathbf{x}\|_0 \\ subject\ \ to\ \ \boldsymbol{\Theta}\cdot\mathbf{x} &= \mathbf{y} \end{aligned} \tag{3-6}$$

but this problem is NP-hard [8] which means that there is no tractable algorithm that can solve it for any $\boldsymbol{\Theta}$ and $\mathbf{y}$. On the other hand, Donoho [9] proposed to move the problem to the ℓ_1 norm minimization as follows:

$$\begin{aligned} \hat{\mathbf{x}} &= arg\min_x \|\mathbf{x}\|_1 \\ subject\ \ to\ \ \boldsymbol{\Theta}\cdot\mathbf{x} &= \mathbf{y} \end{aligned} \tag{3-7}$$

because, although the system of equations is massively underdetermined, ℓ_1 minimization and the sparse solution coincide, when the result is sufficiently sparse and the matrix sufficiently incoherent. Besides, (3-7) is a convex optimization problem. As a result, for the ℓ_1 norm minimization, there are plenty of algorithms like basis pursuit, orthonormal matching pursuit etc.

Since, in radar data there is thermal noise, the measurements become:

$$\mathbf{y} = \boldsymbol{\Phi}\cdot\mathbf{s} = \boldsymbol{\Phi}\cdot(\boldsymbol{\Psi}\cdot\mathbf{x}+\mathbf{z}) = \boldsymbol{\Theta}\cdot\mathbf{x}+\boldsymbol{\Phi}\cdot\mathbf{z} \tag{3-8}$$

where $\mathbf{z}$ is complex Gaussian noise with zero mean and variance γ , $p(\mathbf{z}|\gamma) \propto exp(-|\mathbf{z}|^2/\gamma)$ [12]. When the sparsity of $\mathbf{x}$ is formalized by a multivariate Laplace prior $p(\mathbf{x}|\lambda)$, $p(\mathbf{x}|\lambda) \propto exp(-\lambda|\mathbf{x}|_1)$, the maximum a posteriori (MAP) estimator of x, written as:

$$\mathbf{x}_{MAP} = arg\min_x \|\mathbf{y}-\boldsymbol{\Theta}\cdot\mathbf{x}\|_2^2 + h\|\mathbf{x}\|_1 \tag{3-9}$$

gives the usual SSP from CS with the l_1-norm $\|\mathbf{x}\|_1$ promoting the sparsity and the l_2-norm $\|\mathbf{y}-\boldsymbol{\Theta}\cdot\mathbf{x}\|$ for minimizing the errors, together with a control parameter h that balances between the two tasks ([9], [12]). In that form of SSP, the constant h depends on the variance of the noise γ and the sparsity parameter since $h = \gamma\lambda$ [12]. When it is related to the GLRT, then h becomes known and related to the probability of false alarm P_{fa} [13] from $h = \sqrt{-\gamma \ln P_{fa}}$.

Chapter 4

Data Acquisition Schemes

4-1 Introduction

In this chapter, we will analyze four architecture schemes of data acquisition in radar systems with CS. We first clarify the basic details of our system and then, state our scenario case with an incoming signal from a target which reflects the transmitted signal. In order to take advantage of the spatial characterization of the signal, we use an array of antenna elements for the reception of the signal. Usually, our purpose is the spatial filtering of that signal in such a way that the signal arriving to the array at a specific angle, can be effectively distinguished among other interfered signals and other targets [14]. Our goal in this thesis is to analyze the way an array of antenna elements receives a signal from a certain angle and how its digital samples are obtained. To do so, we first need to model the incident signal. At first, all transmitted and received analog signals are real sinusoids in the radar front end becoming complex signals in the discrete domain [5]. Therefore, we model the signal as complex so that the incoming signal is represented as the real part of a complex signal. Later on we will treat the signals as complex for the sake of simplicity.

Let us begin by representing a bandpass signal $u(t)$ as:

$$u(t) = x(t) \cdot cos(2\pi f_c t) - y(t) \cdot sin(2\pi f_c t) \tag{4-1}$$

where f_c is the carrier frequency, $x(t)$ and $y(t)$ are the real baseband signals of bandwidth B whose initial phase of the carrier is neglected. Now, we can define the complex baseband equivalent signal

of $u(t)$ as:

$$s(t) = x(t) + jy(t) \tag{4-2}$$

where $x(t) = \mathrm{Re}\{s(t)\}$ is the in-phase component of $u(t)$ and $y(t) = \mathrm{Im}\{s(t)\}$ is the quadrature component of $u(t)$. In practice, we produce them with the Hilbert transform [5]. With these definitions, the transmitted signal can be written as:

$$u_{tr}(t) = \mathrm{Re}\Big\{ s(t) \cdot e^{j2\pi f_c t} \Big\} \tag{4-3}$$

Similarly, the form of the received signal will be

$$u_{rc}(t) = \mathrm{Re}\Big\{ q(t) \cdot e^{j2\pi f_c t} \Big\} \tag{4-4}$$

where the complex baseband signal $q(t)$ will depend on the channel through which $s(t)$ propagates. In particular, if $c(t)$ is the equivalent channel impulse response, which will be the air in our case, and $u_{tr}(t)$ is the transmitted signal through that channel, then $v(t) = u_{tr}(t) * c(t)$. For the rest of the report, we will assume that the received signal is just a delayed version of the transmitted one for simplicity. Thus, we have:

$$u_{rc}(t) = u_{tr}(t-\tau) = \mathrm{Re}\Big\{ s(t-\tau) \cdot e^{j2\pi f_c (t-\tau)} \Big\} \tag{4-5}$$

where τ is the delay caused by the channel i.e. the range of the target.

4-2 Uniform Linear Array

Now that we have modeled the incoming signal at the antenna, we can characterize the antenna array which will be used for the reception of the signal as the reference.

The design of an array of antennas for the achievement of a certain performance involves a trade-off between the geometry of the array, the number of antenna elements, the SNR, the SIR, and a large number of other parameters [14]. In spatial filtering, the most important aspect in array design is the geometry of the array. For the rest of the project, we will focus on a linear array since we intend to resolve only one angular component, as an example. In addition, the distance between each neighboring pair of antenna elements will be equal so we are talking about a ULA.

Suppose that we have a planar wave received by M antennas as shown in Figure 4-1, [15]. The signal captured from each antenna is a delayed version of the one which arrives first at the

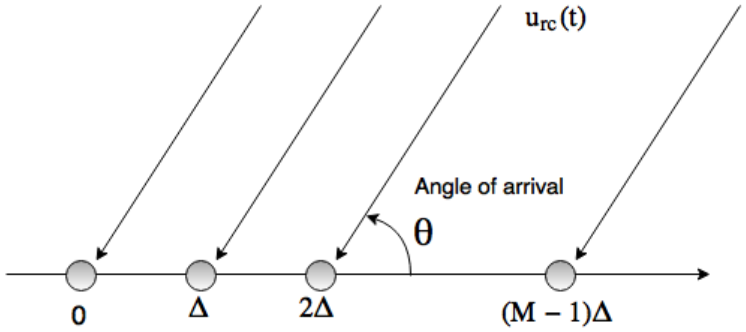

Figure 4-1: Uniform Linear Array.

array [16]. So, we understand that there is a dependence on the point x in space where we capture the signal. As a result, we can write the incident planar wave in the $m-th$ antenna as follows:

$$u_{rc}(t;x_m) := u_{tr}(t-\tau_m) = \mathrm{Re}\Big\{s(t-\tau_m)e^{-j2\pi f_c(t-\tau_m)}\Big\} = \mathrm{Re}\Big\{s(t-\tau_m)e^{-j2\pi f_c\tau_m}e^{j2\pi f_c t}\Big\} \tag{4-6}$$

where $(t;x_m)$ indicates the dependency of the planar wave on space and time since t is the time index which parametrized by x_m which is the position of the antenna and τ_m is the time delay between two antennas. According to the narrowband approximation, when the time delays which are introduced to these signals are much smaller than the inverse of their bandwidth, the delays can be represented by phase shifts only [16]. In other words, through two antenna elements, there is no range cell jump and it means that the signal remains inside the same range resolution cell. Thus, if the complex envelope of the delayed signal received by antenna element m is $s_\tau(t)$, it can be written as :

$$s_\tau(t) = s(t-\tau)\cdot e^{-j2\pi f_c\tau} \simeq s(t)\cdot e^{-j2\pi f_c\tau} \tag{4-7}$$

end equation (4-6) can be rewritten as follows:

$$u_{rc}(t;x_m) := u_{tr}(t-\tau_m) \simeq \mathrm{Re}\Big\{s(t)\cdot e^{-j2\pi f_c\tau_m}e^{j2\pi f_c t}\Big\} \tag{4-8}$$

It is also important to say that the maximal delay is observed between the edges of the antenna array. This distance is called aperture D of the array and is expressed in wavelengths. For narrowband signals with carrier frequency f_c, the corresponding wavelength will be $\lambda = c/f_c$, where c is the wave-propagation speed and equal to the velocity of light. So, if δ_m is the distance between the $m-th$ antenna element from the first one, then $\delta_m = (m-1)\Delta\cdot\lambda$ where Δ is the actual distance between each pair of neighboring antenna elements (given in a number of wavelengths).

Since we have defined the form of the array and the incoming signal $u_{rc}(t)$, we can define the signal as it is captured by the array. If it is assumed that the $m-th$ antenna element introduces a gain pattern $g_m(\theta)$ which is a function of the angle of arrival θ, then the output of the $m-th$ antenna element is given by:

$$y_{RF,m}(t) = g_m(\theta) \cdot u_{rc}(t;x_m) = g_m(\theta) \cdot u_{tr}(t-\tau_m) \tag{4-9}$$

Assuming that each antenna element is identical in the received signal, we can write the gain pattern as $g_m(\theta) = g(\theta)$. In addition, the complex equivalent will be used from the very beginning of the chain although in actual radar systems, it is real up to Hilbert transformation in the discrete domain at the baseband. Keeping the captured signal as real, would make the calculations complicated and less clear. By implementing this simplification, the sampling rate in the end will be doubled because of the complex baseband equivalent and the variance of the LNAs will be doubled, too. By leveraging equations (4-8) and (4-9), we have:

$$y_{RF,m}(t) = g(\theta) \cdot u_{tr}(t-\tau_m) = g(\theta) \cdot s(t) \cdot e^{-j2\pi f_c \tau_m} \cdot e^{j2\pi f_c t} \tag{4-10}$$

If we take a look again at Figure 4-1, then we can express the delays τ_m with respect to the position of the $m-th$ antenna element by using geometry and the conventional definition of motion as follows:

$$\begin{gathered} \tau_m = -\frac{\delta_m sin(\theta)}{c} = \frac{(m-1)\Delta\lambda sin(\theta)}{c} \\ so \;\; we \;\; have \;\; 2\pi f_c \tau_m = -2\pi(m-1)\Delta sin(\theta) \end{gathered} \tag{4-11}$$

Finally, we can write the received signal as follows:

$$y_{RF,m}(t) = g(\theta) u_{tr}(t-\tau_m) = g(\theta) s(t) e^{j2\pi(m-1)\Delta sin(\theta)} e^{j2\pi f_c t} \tag{4-12}$$

Collecting all the signals into a vector $\mathbf{y}_{RF}(t)$, we obtain from (4-12):

$$\mathbf{y}_{RF}(t) = \begin{bmatrix} 1 \\ e^{j2\pi\Delta sin(\theta)} \\ \vdots \\ e^{j2\pi(M-1)\Delta sin(\theta)} \end{bmatrix} g(\theta) \cdot s(t) \cdot e^{j2\pi f_c t} := \mathbf{a}(\theta) \cdot s(t) \cdot e^{j2\pi f_c t} \tag{4-13}$$

where $\mathbf{a}(\theta)$ is the array response vector i.e. the response of the array to a planar wave coming from an angle of arrival θ and contains the gain $g(\theta)$ of the antenna element. Here, we must point out that the

phase shifts $2\pi\Delta sin(\theta)$ lie in the interval $[-2\pi\Delta, 2\pi\Delta]$. We can easily see that if $\Delta > \frac{1}{2}$ wavelengths, then this interval extends beyond $[-\pi, \pi]$ and then, we can see that several values of θ give the same phase shifts. Thus, the maximum inter-element spacing is $\frac{1}{2}$ wavelengths and the radar aperture, for a certain number of antenna elements M of our choice, will be $D = (M-1)\Delta$ wavelengths.

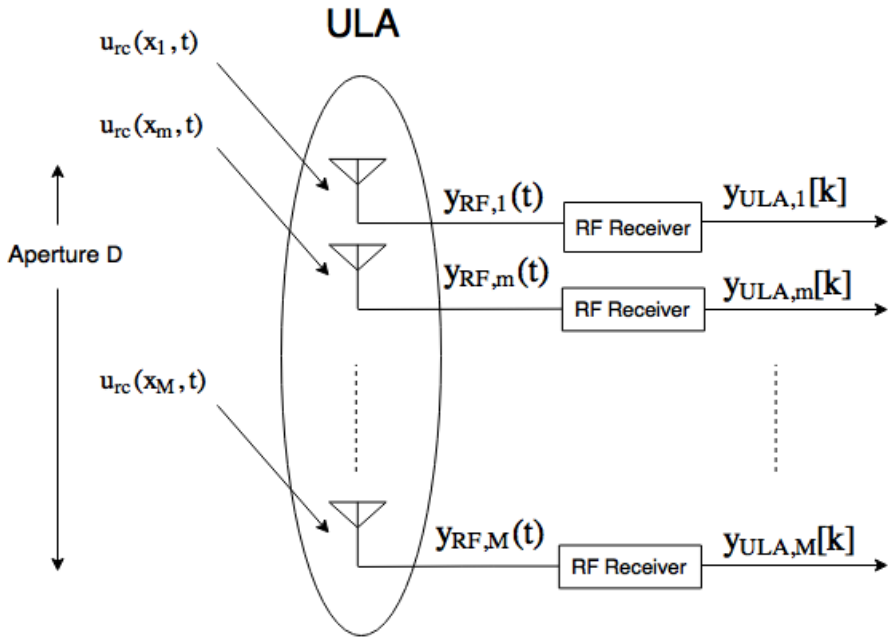

Figure 4-2: Uniform linear array of antenna elements.

Since the incident planar wave to the antenna array have been modeled, we can move to the different stages of the radar system. The RF signal which we will use, will be the superheterodyne receiver we described in Chapter 1 which downconverts the input signal to baseband through two mixing procedures and then, digitizes it by sampling it at the Nyquist rate. At the end, the output will be a discretized version $y_{ULA,i}[k]$ for $i = 1, ..., M$ at one time instance k as shown in figure (4-2). So, the output vector we obtain from the ULA has the form:

$$\boldsymbol{y}_{ULA} = \mathbf{a}(\theta) \cdot s + \mathbf{n} \tag{4-14}$$

where $\mathbf{n}$ is the noise which is caused by the components of the RF receiver of the M channels and is complex Gaussian, zero mean additive noise $CN(\mathbf{0}, \gamma \mathbf{I}_M)$ with noise covariance matrix $R_{MM} = \mathbf{I}_M$. For the rest of the thesis, we will focus on spatial sampling where in each period, we obtain one sample from each antenna element. So, since the distance between each pair of neighboring antenna elements is the same and equal to half of a wavelength, we are talking about spatially uniform sampling at Nyquist rate. If we place each pair of neighboring antenna elements closer than half of a

wavelength, then we will have oversampling whereas, if we place them more than that, we will have undersampling.

Lastly, in order to fully describe the aperture size of the radar system, we have to follow some steps which will lead to an accurate characterization of the architecture. The reason we are doing this, is that we have to be precise and consistent in building the reference blocks to be used in all the other radar receiving architecture schemes which we will compare.

At first, let us assume that the radar system operates by transmitting pulses in a specific frequency band. If f_c is the operating frequency, then the wavelength is given by $\lambda = \frac{c}{f_c}$. Depending on the type of radar system, the type of antenna elements varies with their physical size d. Intuitively, if we also take a look at Figure 4-3, we understand that in a ULA consisting of M antenna elements with a space of Δ between them, the total aperture D will be:

$$D = \frac{d}{2} + (M-1)\cdot\Delta\cdot\lambda + \frac{d}{2} = (M-1)\cdot\Delta\cdot\lambda + d \tag{4-15}$$

So, if we are going to use half-wavelength dipole antennas, their length will be $d = \frac{\lambda}{2}$ and if the distance Δ will be $\frac{1}{2}$, then the total aperture will be $D = M\cdot\frac{\lambda}{2}$.

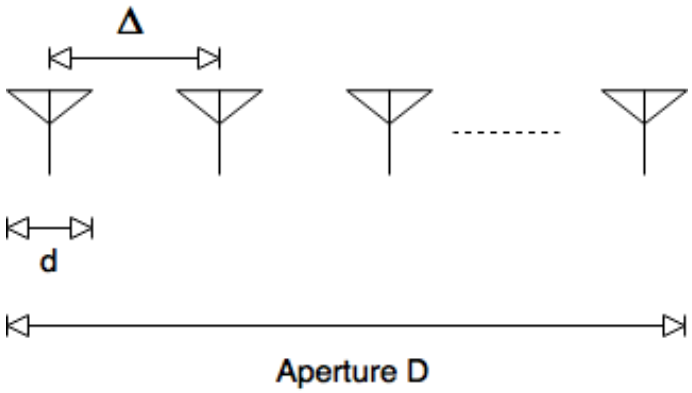

Figure 4-3: Representation of distances in a ULA.

Since we have clarified the type of antenna which will be used, we can calculate also the gain $g(\theta)$ of each antenna element which is given by the equation [2]:

$$g(\theta) = \frac{4\pi\cdot A_{eff}(\theta)}{\lambda^2} \tag{4-16}$$

where $A_{eff}(\theta)$ is the effective area of the antenna element and it is expressed as $A_{eff}(\theta) = \eta A(\theta)$ where $A(\theta)$ is the maximum effective aperture and η is the antenna aperture efficiency which depends

on the distribution of the illumination across the aperture. In practice, the effective area A_{eff} of an antenna is the value corresponding to the direction of maximal gain. Also, linear antennas are fixed-gain antennas so, since we will use a halfwave dipole, we can write the gain as:

$$g = \frac{4\pi \cdot A_{eff}}{\lambda^2} \tag{4-17}$$

Signal and Noise power

In Chapter 1 we have calculated the total gain and noise figure of each individual channel of a ULA but, if we want to fully describe the influence of each channel to the incident signal, we have to describe also the signal and the noise power in both input and output of the architecture.

As we have already mentioned, the signal incident to the array, is captured by a uniform linear array of antenna elements. This signal is coming from a target in the field of view of the radar system and has a power density which is given by the radar equation [1]:

$$P_{inc} = \frac{P_T \cdot G_T \cdot \sigma}{(4\pi R^2)^2} \tag{4-18}$$

where P_T is the transmitted power, G_T is the gain of the transmitting antenna, σ is the RCS of the target and lastly, R is the distance of the target. This power density of the incident wave will be the same for all the architectures that will be analyzed later. As a result, the amount of power captured by the $m-th$ antenna element and is the input to the ULA, is given by:

$$P_{in,m}^{ULA} = A_{eff} \cdot P_{inc} = \frac{P_T G_T g \lambda^2 \sigma}{(4\pi)^3 R^4} \tag{4-19}$$

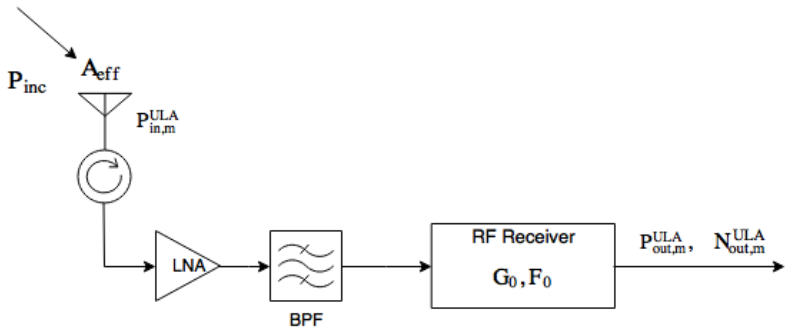

Figure 4-4: Equivalent channel of a ULA.

Concerning the output power signal and noise power, as shown in figure 4-4, we compute their maximum ratio being the SNR after matched filtering (MF). As a result, if the output of MF in the model 4-14 is given by:

$$y_{ULA}^{MF} = \|\mathbf{a}(\theta)\|^2 s + \mathbf{a}(\theta)^H \mathbf{n} \tag{4-20}$$

then we can compute the total output signal and noise power, along with the total output SNR as follows:

$$P_{out}^{ULA} = \left| \|\mathbf{a}(\theta)\|^2 s \right|^2 = |s|^2 \|\mathbf{a}(\theta)\|^4 = M^2 \cdot g^4 |s|^2 \tag{4-21}$$

$$N_{out}^{ULA} = E\left\{ \|\mathbf{a}(\theta)^H \cdot \mathbf{n}\|^2 \right\} = E\left\{ \left| \sum_{m=1}^{M} a_m(\theta) \cdot n_m \right|^2 \right\} = \sum_{m=1}^{M} |a_m(\theta)|^2 E\left\{ |n_m|^2 \right\} = M \cdot g^2 \cdot \gamma \tag{4-22}$$

$$SNR_{out}^{ULA} = \frac{P_{out}^{ULA}}{N_{out}^{ULA}} = \frac{M^2 \cdot g^4 |s|^2}{M \cdot g^2 \cdot \gamma} = M \cdot \frac{g^2 |s|^2}{\gamma} \tag{4-23}$$

ULA is an architecture which has the highest output SNR and performance due to the large number of antenna elements. The drawback is that in cases where the signal of interest has multiple frequency bands or its bandwidth is really high (above 10GHz), its sampling is limited by two main problems. The first one is the high power consumption when the existing modern ADCs are used for inputs of bandwidth 10 GHz or more. The second problem comes from the need of storage when we try to sample this kind of signals at Nyquist rate. For example, even if we could have a low power ADC of 10GHz input bandwidth, we must sample it with 25 GSa/s which demands a huge amount of memory. So, most of the acquired data, since only a really small fraction of them contain the useful information, are redundant and they are thrown away after reception in order to reduce the storage and transmission requirements of the respective applications.

In the following, the CS data acquisition is presented which omits these two problems, when it is known that the signal of interest is sparse under known transformations. This field of study is called compressive sensing which has been introduced in Chapter 3. The sampling of multiband signals can be done simply by using multiple channels, each one of them implementing different downconvertion and filtering but this can happen only when the bands are known. In the opposite case where we do not know the position and the bandwidth of the signal's bands, we can use CS architectures. A usual choice of receiver is called Multiband Wideband Converter (MWC) described in [17] and [18]. The MWC processes the input multiband signal by using m simultaneous channels and at each one of them, the signal is multiplied by a periodic function, which is a pseudorandom sequence, and then, it is low-pass filtered and sampled uniformly at rate twice the cut-off frequency

of the respective filter. The mixing operation scrambles the spectrum of the input signal, such that a portion of the energy of all bands appears in baseband.

In the following sections, three different data acquisition architectures for a radar system with CS are presented, namely, multi-coset sampling, analog-to-information converter and uniform linear array of metamaterial surface antennas, where the compression of the incoming signals takes place at three different spots in the radar chain: before, after and at reception, respectively.

4-3 Multi-coset Sampling

The first CS architecture we are going to analyze is called Multi-Coset sampling [19, 20]. In MC sampling, the method we are using is a modified version of MWC. Here the MC sampler consists of P parallel channels that sample the input signal at a really low rate but with different time offsets like Figure 4-5, [19]. These time offsets are chosen from a sampling pattern within an interval of one period. In every multi-coset sampling period, P out of L samples are chosen (where L is the number of samples that would have been obtained by sampling at Nyquist rate) and they are defined as sampling pattern. Thus, we can characterize MC sampling as a sub-Nyquist rate, undersampling technique in

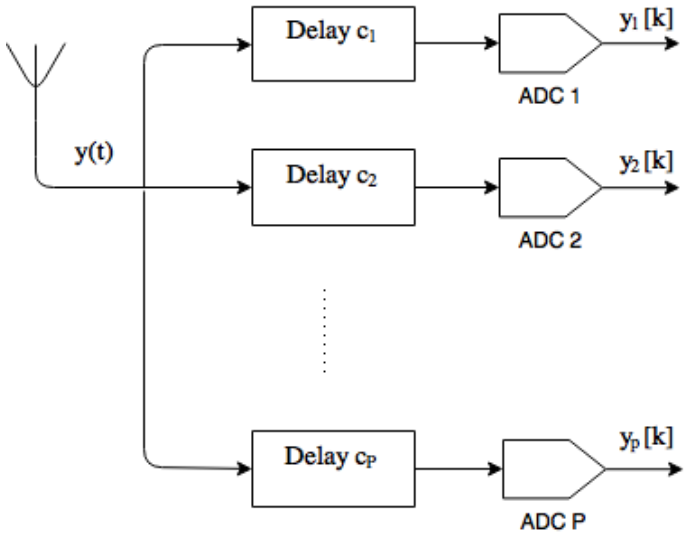

Figure 4-5: Multi-coset Sampling in Time domain.

which an arbitrary non-uniform sampling combination is periodically applied to an RF signal.

Mathematically speaking, when the signal enters the MC sampler, it is split into periods of L samples, where L is the multi-coset sampling period. Then, each channel i introduces a different

time delay of c_i samples where $c_p \in \{0,1,...,L-1\}$, $1 \leq P < L-1$ and $C = \{c_1, c_2, ..., c_p\}$ is the multi-coset sampling pattern which is applied at each MC period. Lastly, the procedure is followed by an integrate-and-dump device with period LT (thus with rate equal to $1/L$ times the Nyquist rate). As a result, we can rewrite the digitized samples as follows:

$$y_p[k] = \int_{(kL+c_p)T}^{(kL+c_p+1)T} y(t)\mathrm{d}t \tag{4-24}$$

where $T = \frac{1}{2 \cdot f_{max}}$ is the Nyquist period. Lastly, We understand that in this architecture, we perform *compressive sensing before reception* since we choose to keep some of the samples captured at Nyquist rate.

Now that we have defined MC sampling in the time domain, we apply this architecture to our case which is going to be spatial sampling of a planar wave given by equation (4-12). In spatial sampling, we take samples from each antenna element and when these are spaced by half of a wavelength then we are talking about Nyquist rate. So, since for MC in time domain we select P out of L samples obtained at the Nyquist rate, the MC pattern in spatial domain will be simply a selection of P out of M antenna elements.

As we mentioned before, the antenna array of a ULA consists of M antenna elements equally spaced by Δ wavelengths between them. Thus, in this case, we will choose to capture the incident signal only from P antenna elements. The space between them will be given by the MC pattern. In addition, in order to be able to compare this architecture with a ULA, we must clarify that the radar aperture D must remain the same. Thus, if $y_{RF,m}(t)$ for $m = 1,2...,M$ is the incident signal to the array captured by M antenna elements, then we select $y_{MC,p}(t)$ where $p = 1,2...,P$ are the channels after selection and $y_{MC,p}[n]$ will be the digitized samples after the RF receiver. Again, a superheterodyne receiver will be used as an RF receiver. So, an equation which can describe the equivalence is given as follows:

$$y_{MC,p}(t) = y_{RF,c_p}(t) \tag{4-25}$$

where $c_p \in \{0, \Delta, 2\Delta, ..., D-\Delta\}$ obtained from the MC pattern $C = \{c_1, c_2, ..., c_p\}$. Similarly, we can state the equivalence in matrix form using the discretized data from a ULA and introducing the additive complex Gaussian noise of P channels $\mathbf{n}_{MC} \sim CV(0, \gamma \mathbf{I}_\mathrm{P})$ with noise covariance matrix $\mathbf{R}_{PP} = \gamma \mathbf{I}_\mathrm{P}$, as follows:

$$\mathbf{y}_{MC} = \mathbf{H}_{MC} \cdot \mathbf{y}_{RF} + \mathbf{n}_{MC} \tag{4-26}$$

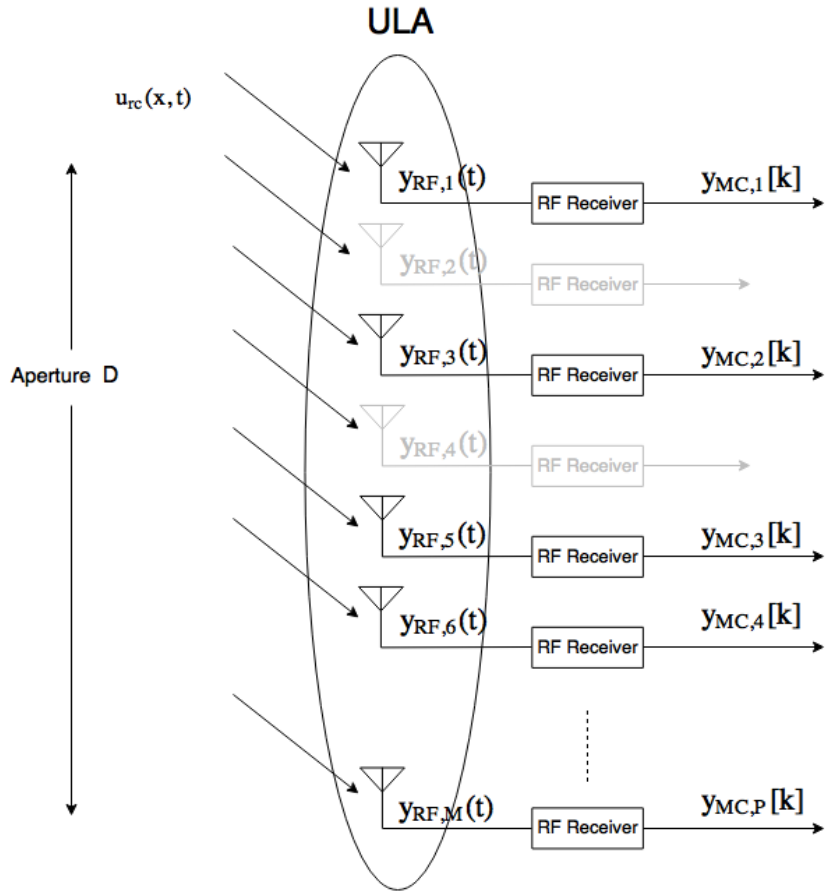

Figure 4-6: Multi-coset Sampling in Spatial domain

where $\mathbf{H}_{MC}$ is the PxM selection matrix which contains value $[\mathbf{H}_{MC}]_{i,j} = 1$ for $i = 1,...,P$ and $j = c_1,...,c_p$ with $c_1 = 0$ and $c_p = D - \Delta$ because we want the aperture to be the same as the one of the ULA. The summarized function of multicoset sampling, can be viewed in Figure 4-6.

Lastly, we can write the output of the array in a similar way like equation (4-14) by using the array response vector as follows:

$$y_{MC,p} = g \cdot s \cdot e^{j2\pi c_p \Delta sin(\theta)} + n_{MC,p} \tag{4-27}$$

Collecting all the signals into a vector $\mathbf{y}_{MC}$, we can write:

$$\mathbf{y}_{MC} = \begin{bmatrix} 1 \\ e^{j2\pi c_1 \Delta sin(\theta)} \\ \vdots \\ e^{j2\pi (P-1)\Delta sin(\theta)} \end{bmatrix} g \cdot s(t) + \mathbf{n}_{MC} \tag{4-28}$$

So, if

$$\mathbf{a}_{MC}(\theta) = \begin{bmatrix} 1 \\ e^{j2\pi c_1 sin(\theta)} \\ \vdots \\ e^{j2\pi(P-1)\Delta sin(\theta)} \end{bmatrix} g \tag{4-29}$$

then the final vector of the Multi-coset architecture will be:

$$\mathbf{y}_{MC} = \mathbf{a}_{MC}(\theta) \cdot s + \mathbf{n}_{MC} \tag{4-30}$$

Signal and Noise power

For the calculation of the signal and noise power, it is obvious that the input and output power per each channel will be the same. The difference lies in the total output power of the MC sampling architecture since the number of outputs are less.

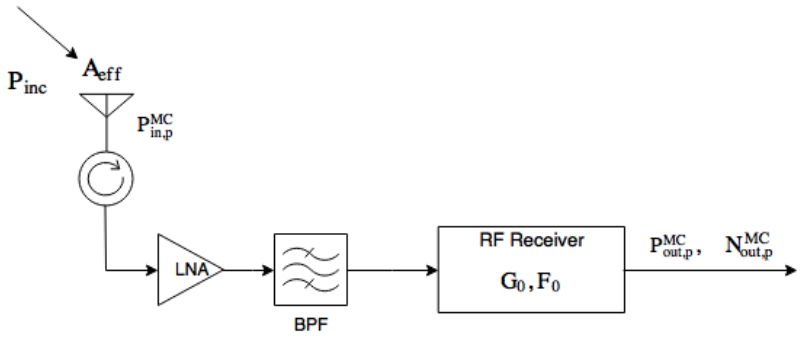

Figure 4-7: Equivalent channel of a ULA.

As a result, by using model (4-30), we can easily compute the output signal and noise power, and also the output SNR as follows:

$$y_{MC}^{MF} = \|\mathbf{a}_{MC}(\theta)\|^2 s + \mathbf{a}_{MC}(\theta)^H \mathbf{n}_{MC} \tag{4-31}$$

$$P_{out}^{MC} = \left| \|\mathbf{a}_{MC}(\theta)\|^2 s \right|^2 = |s|^2 \|\mathbf{a}_{MC}(\theta)\|^4 = P^2 \cdot g^4 |s|^2 \tag{4-32}$$

$$N_{out}^{MC} = E\left\{ \|\mathbf{a}_{MC}(\theta)^H \cdot \mathbf{n}_{MC}\|^2 \right\} = E\left\{ \left| \sum_{p=1}^{P} a_{MC,p}(\theta) \cdot n_{MC,p} \right|^2 \right\} = \sum_{p=1}^{P} |a_{MC,p}(\theta)|^2 E\left\{ |n_{MC,p}|^2 \right\} = P \cdot g^2 \cdot \gamma \tag{4-33}$$

$$SNR_{out}^{ULA} = \frac{P_{out}^{ULA}}{N_{out}^{ULA}} = \frac{P^2 \cdot g^4 |s|^2}{P \cdot g^2 \cdot \gamma} = P \cdot \frac{g^2 |s|^2}{\gamma} \tag{4-34}$$

which is actually the SNR after MF in the model (4-30), as MF is the optimum-SNR basis for any signal processing.

4-4 Analog-to-Information Converter

Analog-to-information converter (AIC) [21–23] is a standard framework of data acquisition in CS [8], [9]. The extraction of the information is operated by a matrix Φ which replaces the conventional sampling and reconstructs the input signal with back-end digital signal processing. The classic AIC scheme exploits spread-spectrum techniques from communication theory [24, 25] where an analog mixture in the front end of the application, aliases the spectrum in such a way that a small portion from each band appears at low frequencies (baseband). In other words, again it is a similar scheme as MWC and MC sampling. So, there is a mixing in analog domain, then we will have a linear system with more equations than unknowns and the recovery of the sparse multiband signal is performed efficiently [17]. Intuitively, each output will be a linear system of the unknowns and the number of outputs depends on the number of active frequency bands of the signal.

More specifically, the received signal enters the receiver and it is demodulated by a multiplication with a mixing function $p_c(t)$ which is T_p periodic. As we mentioned before, a small portion of each band is moved to baseband so the signal is filtered by passing through a low-pass filter with cut-off frequency $\frac{1}{2T_s}$ and then sampled at frequency $\frac{1}{T_s}$ which is sufficiently low. Here, we should point out that we are using a pseudorandom sequence as a mixing function, which alternates between ± 1 at or faster than the Nyquist frequency of the input signal. That is because we just need to move the frequency band to baseband. A block scheme representation of the AIC in the time domain is shown in Figure 4-8, [17].

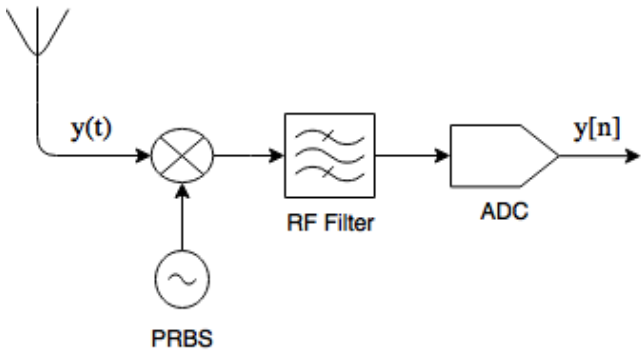

Figure 4-8: AIC in Time domain.

In a similar way, we can perform compression in spatial domain. At first, we must point the obvious differences. Since we have an array of antenna elements, we capture phase shifted versions of

the incident planar wave so we are going to have multiple channels but less in number than in ULA. Secondly, the multiplication will be among the mixing function and the respective signal coming from the array. Thirdly, the mixing function will not be a pseudorandom binary sequence but phase shifts picked up from a uniform distribution. Lastly, the mixing function will not be periodic since the method is applied to each channel at one time instance. As a result, we are not doing channel selection like we did in the previous case (MC sampling). What we are doing here can be considered as a random placement of the antenna elements inside a constant aperture D, introducing random phase shifts at each output.

A detailed representation of the AIC in spatial domain is presented in Figure 4-9. More specifically, the signals captured by the antenna elements, first pass through LNAs because when the signal is captured, it is very weak and we can't process it. That is why we use an LNA directly after the antenna elements. Then, a BPF cuts off the out of band signals and after that, the AIC block performs the spatial mixing. This is done by introducing random phase shifts to each branch and then, summing them up to one output. Thus, by introducing random phase shifts we get another output until we have a sufficient number of outputs which can give us a compressed version of the signal. As a result, we have $P < M$ outputs.

Mathematically speaking, if $y_{RF,m}(t)$ is the signal captured by the $m-th$ antenna element, then after the first stage of LNAs, we will have:

$$y'_{RF,m}(t) = y_{RF,m}(t) + n_{LNA,m}(t) \quad for \;\; m = 1,...,M \tag{4-35}$$

As we can see, we now have additive noise in our signal model. This is happening because the LNAs may amplify the signals but also, they amplify the noise which is embedded in them. After that, the AIC can be described by a matrix $\mathbf{H}_{AIC}$ which introduces the phase shifts to each channel and sums them up. By iteratively implementing the same procedure but with different phase shifts, we get multiple outputs. So, the whole procedure can be summed up as follows:

$$\mathbf{y}_{RF,AIC}(t) = \mathbf{H}_{AIC} \cdot \mathbf{y}'_{RF}(t) \tag{4-36}$$

where

$$\mathbf{H}_{AIC} = \frac{1}{\sqrt{P}} \begin{bmatrix} e^{j\phi_{1,1}} & e^{j\phi_{1,2}} & \dots & e^{j\phi_{1,M}} \\ e^{j\phi_{2,1}} & e^{j\phi_{22,2}} & \dots & e^{j\phi_{2,M}} \\ \vdots & & \dots & \\ e^{j\phi_{P,1}} & e^{j\phi_{P,2}} & \dots & e^{j\phi_{P,M}} \end{bmatrix} \tag{4-37}$$

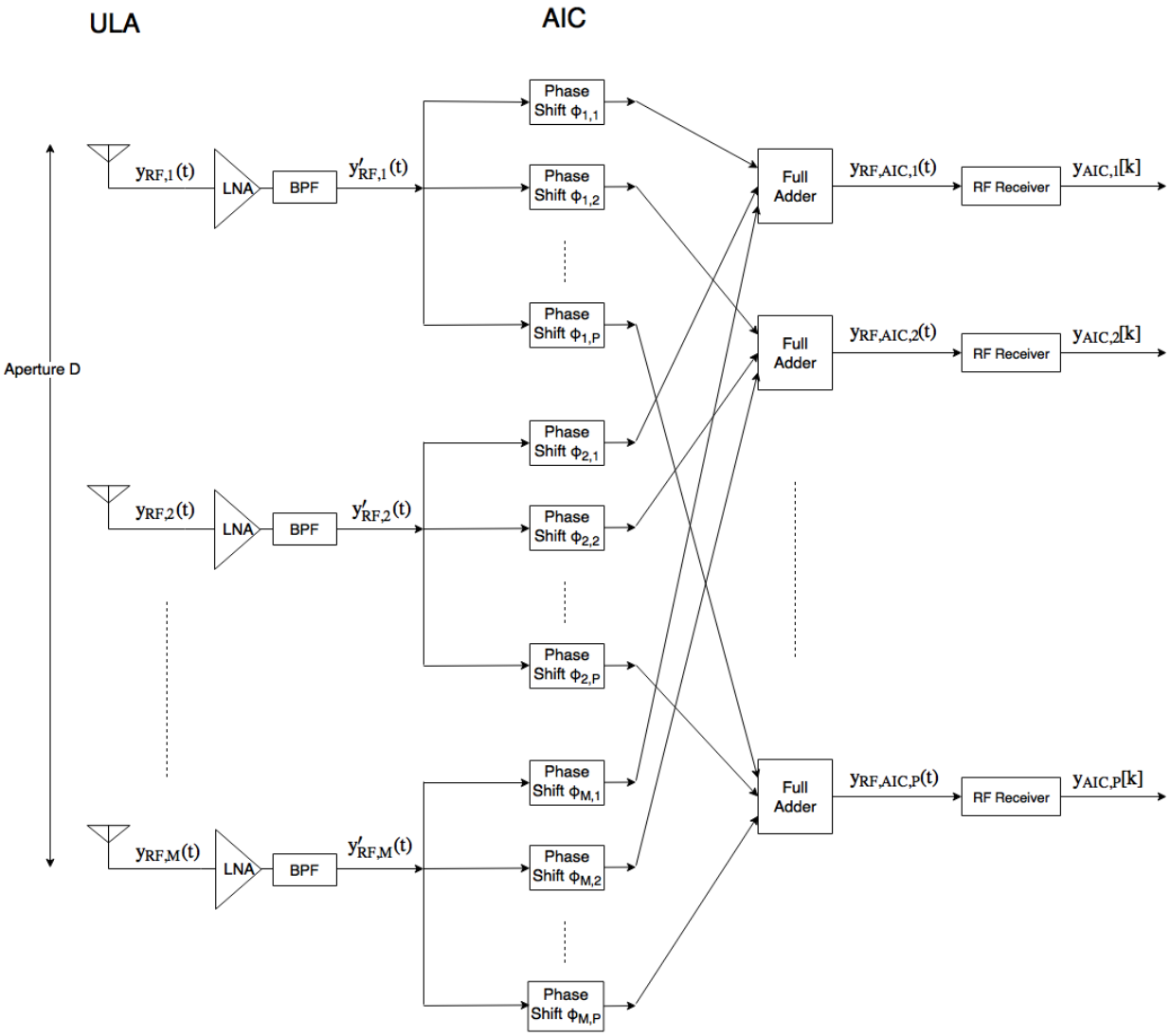

Figure 4-9: AIC in Spatial domain.

The matrix $\mathbf{H}_{AIC}$ is a random PxM matrix where the random phase shifts $\phi_{i,j}$ are digitized i.i.d. drawn from a uniform distribution i.e. $\phi_{i,j} = 2\pi r_{i,j}$ where $r_{i,j} \sim \mathrm{U}(0,1)$ so, $\phi_{i,j} \in \mathrm{U}[0,2\pi)$. In addition, the constant $\frac{1}{\sqrt{P}}$ is used because each $y_{RF,m}$ is split to P branches (with phase shifts) as shown in Figure 4-9. The number of possible different random phase shifts depends on the number of bits of the respective phase shifter. So, for a 8-bit phase-shifter, the number of different values will be 2^8.

Lastly, we can describe the behavior of the whole system by representing the whole procedure of AIC as a matrix like in equation (4-35) by taking a look at Figure 4-9. In other words, we can write:

$$\mathbf{y}_{AIC} = \mathbf{H}_{AIC} \cdot \mathbf{y}'_{RF} \cdot e^{-j2\pi fct} + \mathbf{n}_P = \mathbf{H}_{AIC} \cdot \mathbf{a}(\theta) \cdot s + \mathbf{H}_{AIC} \cdot \mathbf{n}_{LNA} + \mathbf{n}_P \tag{4-38}$$

where $\mathbf{n}_P$ is the noise introduced by P RF receivers to the output signal. Observing equation 4-38, it is

obvious that whatever the system does to the incident signal, the same happens to the noise caused by the LNAs. The output vector of the AIC architecture consists of two terms. The first one means that the signal power will be preserved because of the RIP. From the theory of compressive sensing, the sensing matrix has to be as orthogonal as possible which means that its columns are nearly orthogonal unit vectors. This also means that the RIP must be preserved as introduced in Chapter 3-3-1. In particular, a sensing matrix, which in our case is the normalized matrix $\mathbf{H}_{AIC} \cdot \mathbf{A}(\theta)$, satisfies the RIP if there exists a restricted isometry constant ε, $0 < \varepsilon < 1$, such that:

$$(1-\varepsilon)\|\mathbf{s}\|_2^2 \leq \|\mathbf{H}_{AIC} \cdot \mathbf{A}(\theta) \cdot \mathbf{s}\|_2^2 \leq (1+\varepsilon)\|\mathbf{s}\|_2^2 \tag{4-39}$$

for every K-sparse signal $\mathbf{s}$. As a result, we understand that asymptotically, this equation will turn to equality and the signal power will be preserved.

On the other hand, the second term is the noise introduced by the LNAs multiplied by the sensing matrix $\mathbf{H}_{AIC}$ plus the noise introduced by the components of the RF receiver. This matrix has dimensions PxM which is a fat matrix so it increases the noise power and the variance of the noise in each channel becomes $\gamma_{AIC} = \frac{M}{P} \cdot \gamma$ and $M/P > 1$. In addition, the effect of the noise $\mathbf{n}_P$ of the RF receiver will be smaller than in previous cases since the additional LNA has been placed in the beginning of the chain. So, the RF receiver's components will have a minor effect on the overall thermal noise.

All in all, in order to create a complete equation which describes the AIC architecture, we can write:

$$\mathbf{y}_{AIC} = \mathbf{a}_{AIC}(\theta) \cdot s + \mathbf{n}_{AIC} \tag{4-40}$$

where $\mathbf{a}_{AIC}(\theta) = \mathbf{H}_{AIC} \cdot \mathbf{a}(\theta)$ and $\mathbf{n}_{AIC} = \mathbf{H}_{AIC} \cdot \mathbf{n}_{LNA} + \mathbf{n}_P$ with noise covariance matrix $\mathbf{R}_{PP}^{AIC} = \gamma_{AIC}\mathbf{H}_{AIC}^H\mathbf{H}_{AIC} + \gamma'\mathbf{I_P}$.

Signal and Noise Power

At this point, we can develop a way to calculate the signal and noise power of each branch at the output but the problem in this architecture is that the system uses M antenna elements and it compresses the information in $P < M$ outputs so, the calculation of the parameters for each channel is a bit more complicated.

To begin with, we will calculate the signal and noise power of each branch by assuming that it consists of two stages as shown in Figure 4-10. The first is the one where the signal is captured by M antenna elements and randomly phase shifted (AIC block) with total equivalent gain and noise factor per branch G_{eq} and F_{eq} respectively. On the other hand, the second stage is the downconversion and digitization of the signal through the RF receiver but with the deference that the LNA and the BPF are used in the beginning of the chain, so they are excluded from the RF receiver which used in ULA case. At the end, at the calculation of the parameters, we will assume that we have P channels in parallel and each one of them will have the equivalent form of Figure 4-10. In Figure 4-11, G_0 and F_0 are the equivalent gain and noise factor of the superheterodyne receiver of Figure 2-6 which we will use but without the components of the antenna element, the circulator, the LNA and the BPF since in AIC, these components will be placed in the beginning of the chain.

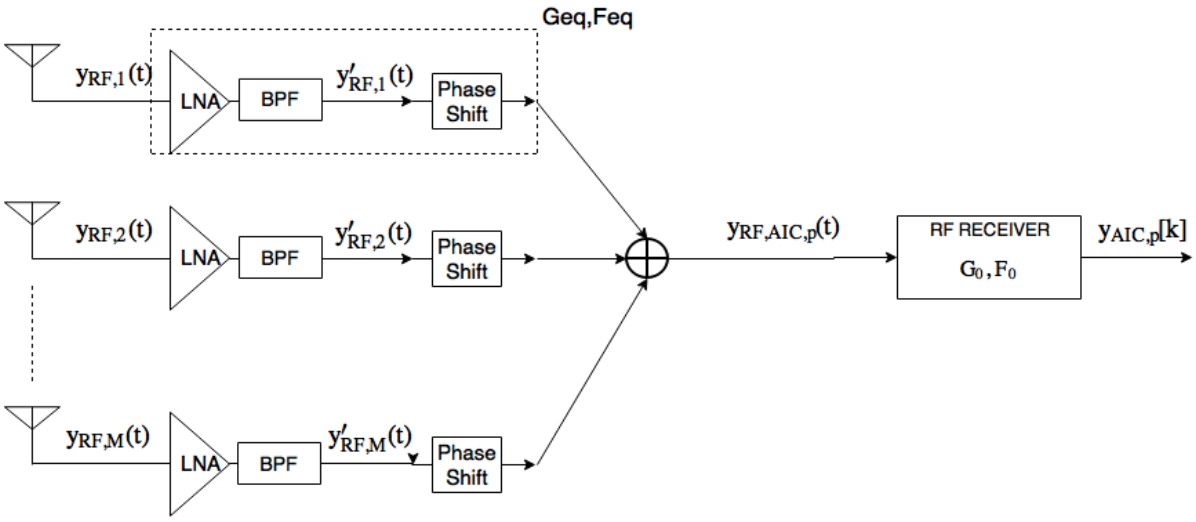

Figure 4-10: Equivalent channel of AIC.

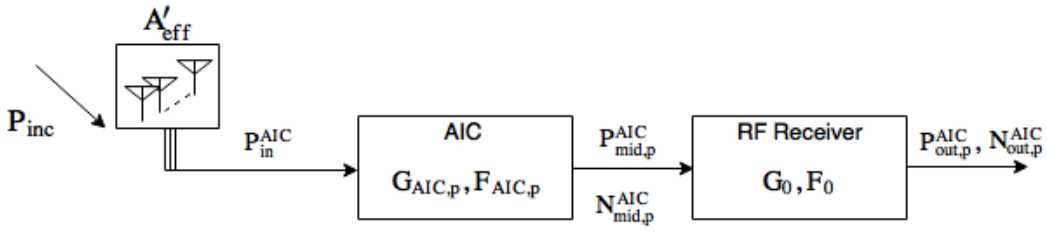

Figure 4-11: Simplified Equivalent channel of an AIC.

For the calculation of the output signal and noise power of the first stage, we will take into

account equation 4-40. More specifically the output signal $\mathbf{y}_{AIC}$ can be approximated as follows::

$$\mathbf{y}_{AIC} = \mathbf{H}_{AIC} \cdot \mathbf{a}(\theta) \cdot s + \mathbf{H}_{AIC} \cdot \mathbf{n}_{LNA} \tag{4-41}$$

At the second stage, the signal containing all the information is driven to the superheterodyne receiver of Figure 2-6, where it is downconverted to baseband and then, sampled at a rate twice as the signal's bandwidth, giving the discretized samples. The procedure of the calculation of all the parameters of the second stage is the same as the one described in Chapter 2. Consequently, the calculation of the output signal and noise power of the total architecture we will use the model 4-40. If we compare these two equations, we can see that the main difference is the noise $\mathbf{n}_P$ introduced by the components of the receive. Though, these components of the RF receiver have negligible effect on the overall noise figure because their position is at the end of the chain so the variance γ' will be very small and can be neglected whereas the variance γ_{LNA} will be almost equal to γ. As a results, if the output of the MF in the model 4-41 is:

$$y_{AIC}^{MF} = \|\mathbf{H}_{AIC} \cdot \mathbf{a}(\theta)\|^2 \cdot s + \big(\mathbf{H}_{AIC} \cdot \mathbf{a}(\theta)\big)^H \mathbf{H}_{AIC} \cdot \mathbf{n}_{LNA} \tag{4-42}$$

then we can compute the maximum output signal and noise power, and SNR after MF as follows:

$$P_{out}^{AIC} = \Big| \|\mathbf{H}_{AIC} \cdot \mathbf{a}(\theta)\|^2 \cdot s \Big|^2 = |s|^2 \cdot \|\mathbf{H}_{AIC} \cdot \mathbf{a}(\theta)\|^4 \tag{4-43}$$

$$\begin{aligned} N_{out}^{AIC} &= E\Big\{ \|\big(\mathbf{H}_{AIC} \cdot \mathbf{a}(\theta)\big)^H \mathbf{H}_{AIC} \cdot \mathbf{n}_{LNA}\|^2 \Big\} \\ &= \gamma \Big(\mathbf{H}_{AIC} \mathbf{a}(\theta) \Big)^H \mathbf{H}_{AIC} \mathbf{H}_{AIC}^H \cdot \mathbf{H}_{AIC} \mathbf{a}(\theta) \\ &= \gamma \|\mathbf{H}_{AIC}^H \mathbf{H}_{AIC} \mathbf{a}(\theta)\|^2 \end{aligned} \tag{4-44}$$

$$SNR_{out}^{AIC} = \frac{P_{out}^{AIC}}{N_{out}^{AIC}} = \frac{|s|^2 \|\mathbf{H}_{AIC} \mathbf{a}(\theta)\|^4}{\gamma \|\mathbf{H}_{AIC}^H \mathbf{H}_{AIC} \mathbf{a}(\theta)\|^2} \tag{4-45}$$

4-5 Metamaterial Surface Antennas

In the last architecture, we are going to implement the same concept as before but in a different manner which is obtained by leveraging metamaterials and compressive sensing. The radar systems we have analyzed so far, consist of an array of antenna elements. In the following scenario, we substitute these antenna elements with metamaterial surfaces in order to take advantage of one specific behavior of them as receivers. This specific behavior which is beneficial in compressive sensing, is the random scattering of the incident wave in their surface. This kind of metamaterial surfaces are

used in applications like synthetic aperture radar [26], computational imaging schemes, surveillance, aeronautics, medical diagnostics and elsewhere [27, 28]. Computational imaging is the field where scene information is acquired by using fewer but less conventional measurements than traditional ones and then the image is reconstructed by computational techniques [29].

In the case where we want to perform applications like through-wall imaging, or ground penetrating radars, we use millimeter waves (30-300GHz) or even submillimeter waves (300 GHz - 1THz) because they can penetrate through materials (visible or infrared) that are opaque at shorter wavelengths. There are many microwave imaging systems that have been developed for that purpose and one of the most recent is synthetic aperture radar (SAR) [26, 30]. In SAR systems, a moving source is electronically steered in order to create a large virtual aperture. This virtual aperture captures signals from the scene from a wide range of angles which can be much larger that the respective of a stationary imaging system. SAR systems consist of highly directive antennas which take the form of phased array antennas or mechanically actuated dishes. Despite the fact that these systems have excellent performance, they suffer from some drawbacks like high energy consumption, large geometric dimensions and they are very expensive. These drawbacks can be omitted by using metasurface aperture antennas which are used to replace the SAR hardware.

Metamaterial apertures are mainly used in computational imaging systems that operate in RF or millimeter-wave frequencies [31–33]. They consist of a large number of subwavelength resonant radiators and each one of them has an assigned resonant frequency which is randomly selected from the operating bandwidth of the receiver. These radiators are etched into a conductive plane which is fed by a waveguide. This waveguide can be a microstrip line when the conducting plane is in one dimension (1D), or a set of two parallel plates if the conducting plane is in two dimensions (2D). A representative figure of both cases is shown in Figure (4-12), [31, 33]. When we apply a signal of different frequencies as excitation, a subset of the etched radiators are excited, depending on the respective assigned resonant frequency, and radiate a distinct radiation pattern into the scene [34]. In other words, they behave like diodes which are integrated into a circuit which switches their states between radiating and non-radiating. In many experiments, horn or probe antennas have been used to capture the backscattered field in order to reconstruct the scene from a set of measurements using computational imaging techniques [35–38]. Thus, by using frequency-diversity, there is no need of mechanical scanning or active electronic components, so the architecture is inexpensive and scalable to very large apertures.

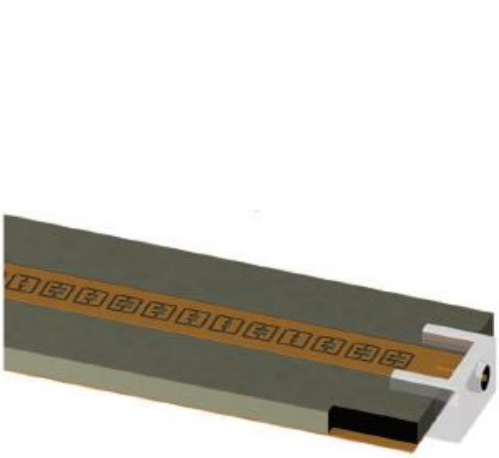

a) 1D Metamaterial Surface

a) 2D Metamaterial Surface

Figure 4-12: Types of Metamaterial apertures.

As we mentioned earlier, the metamaterial aperture consist of subwavelength resonants which are usually complementary electric-inductor-capacitors (cELC) patterned into the upper conductor [31]. Due to their subwavelength geometry, the cELC elements require high-precision printed circuit board (PCB) processes. Also, due to the dispersive nature of the metamaterial elements, large conducting and dielectric losses occur but this research is not the purpose of this thesis project. The important thing we should know is that cELCs control the amplitude and phase of the transmitted signal (when metamaterial surfaces are used for transmission) by changing the resonant frequency and the spectral shape of it [31].

In this project, we are going to use metamaterial apertures to substitute the antenna elements which are used in the previous architecture. To do so, we have to keep in mind several issues which are crucial for the final comparison of the four architectures. At first, the total aperture of the metamaterial surface radar system, has to be equal to the one of the reference case (ULA) and similarly, to the MC and AIC. In addition, this architecture can be characterized as *compression at reception* so, the number of channels which are used will be less than those in the ULA case.

The first problem that we have to face is the number of metamaterial surfaces and the solution lies between two choices. The first one is to use only one metamaterial surface of 1D and length of D. Under this metamaterial surface, we will use a parallel plate waveguide where there will be multiple sensors to capture the signal which is mixed in the analog domain. The number of outputs

is going to be again P < M and these outputs will represent each channel of the antenna array. The second choice is to use multiple metamaterial surfaces which will capture the incident signal with the same aperture of size D. Again, for a fair comparison between the architectures, the number of outputs will be P.

In most of the metamaterial imaging schemes, a metamaterial surface is used to radiate a complicated pattern [29–38] of beam lobes and then collect the backscattered field. In a tranceiver configuration (when the surface is used for both transmit and receive) the backscattered field is detected by the same aperture which produced the field but, this architecture is too complicated. For that reason, usually a low gain waveguide probe antenna Rx is used to measure the backscattered field like figure (4-13). Also, the driving frequency with which the metamaterial surface changes its radiation

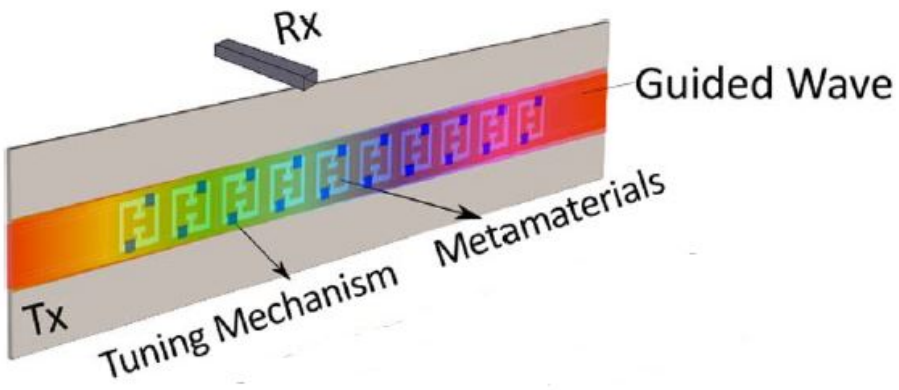

Figure 4-13: Tranceiver scheme of metamaterial surface radar system.

pattern, changes also the backscattered field in such a way that a diverse set of measurement modes is formed. This is something that we want because for image reconstruction scheme which use an arbitrary number of measurement modes, it is essential these modes to be as orthogonal as possible to each other. Thus, a sweeping frequency is a natural choice when we want to introduce diversity to our measurements. Other schemes use mechanical scanning, electronic switching or phasing or even mode-mixing cavities [38, 39]. In radar systems, the received signal consists of multiple frequencies due to moving objects but there is also the case where linearly frequency modulated signals (LFM) are used.

The model we used to describe our ULMA is as follows:

$$\mathbf{y}_{MS} = \mathbf{a}_{MS}(\theta) \cdot s + \mathbf{n}_{MS} = \mathbf{H}_{MS} \cdot \mathbf{a}(\theta) \cdot s + \mathbf{n}_{MS} \tag{4-46}$$

where $\mathbf{n}_{MS}$ is complex Gaussian, zero mean additive noise i.e $n_{MS,p} \sim CN(0, \gamma)$. Accordingly, if the

output of the MF is:

$$y_{MS}^{MF} = \|\mathbf{H}_{MS} \cdot \mathbf{a}(\theta)\|^2 \cdot s + \Big(\mathbf{H}_{MS} \cdot \mathbf{a}(\theta)\Big)^H \mathbf{n}_{MS} \tag{4-47}$$

then we can compute the total output power of the signal, noise power and SNR at the output of the MF as follows:

$$P_{out}^{MS} = \Big|\|\mathbf{H}_{MS} \cdot \mathbf{a}(\theta)\|^2 \cdot s\Big|^2 = |s|^2 \|\mathbf{H}_{MS}\mathbf{a}(\theta)\|^4 \tag{4-48}$$

$$\begin{aligned} N_{out}^{MS} &= E\Big\{\|\Big(\mathbf{H}_{MS} \cdot \mathbf{a}(\theta)\Big)^H \mathbf{n}_{MS}\|^2\Big\} \\ &= \gamma\Big(\mathbf{H}_{MS} \cdot \mathbf{a}\Big)^H \mathbf{H}_{MS} \cdot \mathbf{a} = \gamma\|\mathbf{H}_{MS} \cdot \mathbf{a}\|^2 \end{aligned} \tag{4-49}$$

$$SNR_{out}^{MS} = \frac{P_{out}^{MS}}{N_{out}^{MS}} = \frac{|s|^2\|\mathbf{H}_{MS}\mathbf{a}(\theta)\|^2}{\gamma} \tag{4-50}$$

The modeling of the scattering matrix $\mathbf{H}_{MS}$, the design and the explanation of this particular CS front-end architecture containing metamaterial surface antennas can be found in the annex [40].

Chapter 5

Numerical Results

This chapter contains the simulation results through which we calculate the important parameters , the same way as in in Chapter 2, for each radar front-end architecture of Chapter 4. In addition, we analyze the balance between the complexity and performance of these architectures by using as measures the number of components, the available SNR, the angle of arrival estimation and the mutual coherence.

5-1 Calculation of parameters in Front-End Architectures

As we pointed in Chapter 2, there are some steps we have to follow for the calculation of the three important parameters of a radar front end: the gain, the noise figure and the IP3. At first, we must define the characteristics of the radar system and the incident signal. More specifically, a PD radar system will be used, which operates in C-band where the carrier frequency is $f_c = 5.8GHz$ and a PRF = 10KHz so, the maximum unambiguous range of the radar system, according to equation 2-4, will be $15km$. In a addition, we assume that the incident wave is really weak, with input power $P_{in} = -80dBm$, and a $40MHz$ signal bandwidth.

Parameters	**ADS5410**
Resolution (Bits)	12
Sample Rate (Max) (MSPS)	80
Input channels	1
External Impedance (Z_{in})	50 Ω
SNR (dB)	65
ENOB (Bits)	10.5
SFDR (Spurious-free dynamic range) (dB)	76
SINAD (signal to noise and distortion ratio) (dB)	66
IMD (two tone intermodulation distortion) (dB)	-86
Power Consumption (Typ) (mW)	360
Input Range (V_{p-p})	2
Operating Temperature Range (C)	-40 to 85
Analog Input BW (MHz)	1000
Low-level input voltage (V)	0.5

Table 5-1: Data sheet of ADS5410

5-1-1 Uniform Linear Array of Antennas

The next step is to choose the type of ADC which will be used for the sampling of the RF signal. In our case, since the signal bandwidth is $40MHz$, we choose to use the ADC ADS5410 of TEXAS INSTRUMENTS with the data sheet given in table 5-1. So, substituting the respective values in equation (2-16), we can calculate the noise figure of the ADC and we find $NF_{ADC} = 43.02dBm$.

The way we obtain the gain, noise figure and third-order intercept of each component of a radar receiver is presented in Chapter 2 so, we can calculate the parameters of the whole super-heterodyne receiver which we are going to use in each architecture. In order to ease the calculation, we can use the application of Mathworks with the name "RF Budget Analyzer App" [41] running in MATLAB where we can put all the components of the RF receiver in cascade and then, using the application, we get the per-stage and cascade output power, gain, noise figure, SNR, and IP3 of the system.

Since we have clarified the system's parameters, we add all the components one by one. At

first the signal will be captured by the antenna element with gain 2.15dBi, which is a typical value for a half-wavelength antenna. Since the feed line does not contain electric circuits, it does not introduce any noise figure or IP3. After that, we have to add the circulator since our system is a monostatic radar. For this component, we choose the circulator RFLC-101-3, with gain -1dB, noise figure of 1dB dB [42] and a typical value of IP3 of 37dBm.

Now, we introduce the components of the superheterodyne receiver. At first, we add the first component of a receiver which is always an LNA since it has a low noise figure and high gain. Its gain is 15dB, 3.5 dB noise figure and an IP3 of 26dBm. Along with the LNA, an RF bandpass filter cuts off out of band frequencies. Despite the fact that the application automatically calculates the gain and noise figure values for the filter, they hold for ideal filter and the parameters do not model this loss. For that reason, we use a generic block to model the insertion loss of the filter. For a passive device like this bandpass filter, the gain and the noise figure values will be very low so, we will use some regular values from the literature [43].

The next stages are related to the function of superheterodyne receiver where there are going to be two stages of downconversion. Each part consists of a mixing procedure with a local oscillator to an intermediate frequency, a bandpass filter which cuts off one side of the mixing procedure, a generic block which models the losses of the filter and an amplifier. The second stage will consist of the same components, but with a different mixing frequency. The respective values of the parameters are given in the Figure 5-1. At this point, we should point out that for the case of the mixer, the noise is normally the double sided noise figure, assuming both signal and noise to be present in both RF for the upper and lower sideband ($f_c \pm f_{IF}$) so the noise folding does not impact the noise figure. On the other hand, in the case of the heterodyne receiver, after the mixing procedure only one of the sidebands is useful. As a result, we have a 3dB increase in noise figure, assuming that the conversion gain at both responses is equal. A regular value for the gain of a mixer is 10dB [43].

Additionally, the receiver uses an automatic gain control (AGC) block where the gain varies with the available input power level [44]. For an input power of -80 dB, the AGC gain is at a maximum of 17.5 dB. We put 17.5 dB for available power gain, 4.3 dB for noise figure, and 36 dBm for IP3. Lastly, we have an ADC with the parameters given in Table 5-1. Since we defined the parameters of all the components, we can run the application by introducing all the necessary variables. The interface of the application is indicated in Figure 5-1 and the results are produced automatically from the equations (2-12) and (2-13).

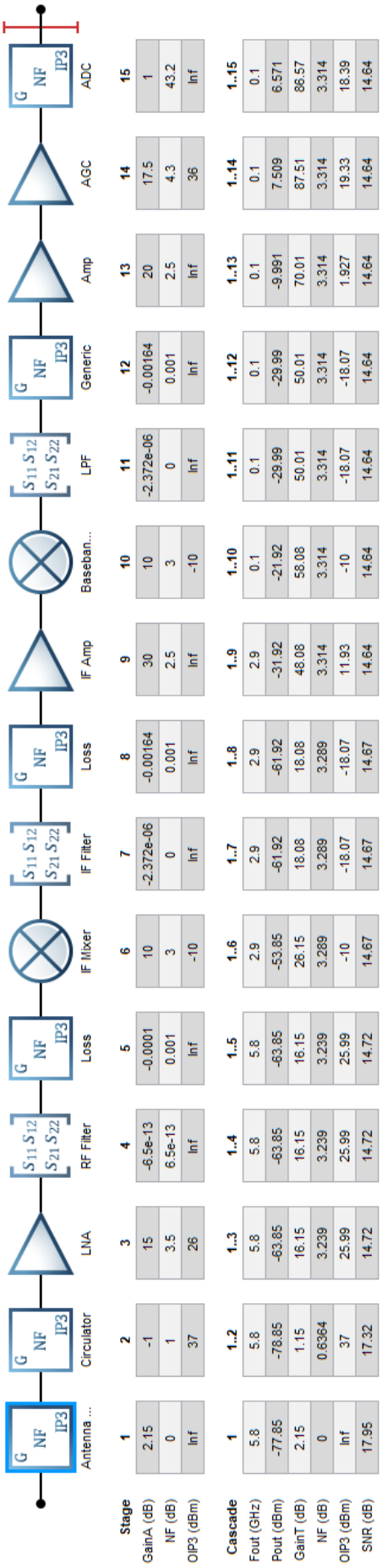

Figure 5-1: Calculated Parameters at each stage of a single channel in a ULA.

At this point, we must say that the total gain, noise figure and IP3 of the superheterodyne receiver can also be calculated from Figure 5-1, if we exclude the component of the antenna element, the circulator and the LNA followed by the BPF. By doing this, we end up with the superheterodyne receiver of Figure 5-2 which can directly be used in any other architecture. In multi-coset sampling, for example, there are less channels than in ULA but both architectures have identical channels.

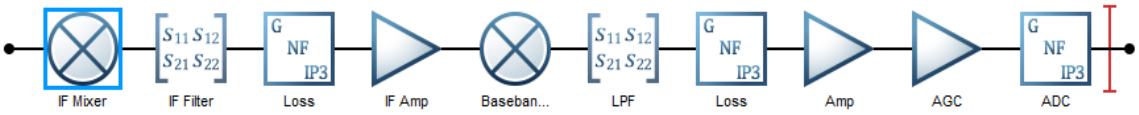

Stage	1	2	3	4	5	6	7	8	9	10
GainA (dB)	10	-2.372e-06	-0.00164	30	10	-2.372e-06	-0.001684	20	17.5	1
NF (dB)	3	0	0.001	2.5	3	0	0.01	2.5	4.3	43.02
OIP3 (dBm)	-10	Inf	Inf	Inf	-10	Inf	Inf	Inf	36	Inf

Cascade	1	1..2	1..3	1..4	1..5	1..6	1..7	1..8	1..9	1..10
Fout (GHz)	2.9	2.9	2.9	2.9	0.1	0.1	0.1	0.1	0.1	0.1
Pout (dBm)	10	1.931	1.929	31.93	41.93	33.86	33.86	53.86	71.36	70.42
GainT (dB)	10	1.931	1.929	31.93	41.93	33.86	33.86	53.86	71.36	70.42
NF (dB)	3	3	3	3.97	3.971	3.971	3.971	3.972	3.972	3.974
OIP3 (dBm)	-10	-18.07	-18.07	11.93	-10	-18.07	-18.07	1.927	19.33	18.39
SNR (dB)	94.95	94.95	94.95	93.98	93.98	93.98	93.98	93.98	93.98	93.98

Figure 5-2: Calculated parameters at each stage of a superheterodyne receiver.

5-1-2 Analog to Information Converter

If we take a look at Figures 4-2, 4-6, 4-9 and 4-14 (refer to the annex), we can see that all the radar front-end architectures use the superheterodyne receiver but in the case of the AIC, we have additional components which introduce the phase shifts and affect the parameters of each channel. As we already have mentioned in Chapter 4, we will calculate the parameters of one channel in AIC by dividing it into two stages, like in Figure 4-10. At first, we will calculate the parameters of the first stage of each channel and since it consists of M parallel branches, we will calculate the values of G_{eq} and F_{eq} and then the total gain and noise figure of the AIC block. So afterwards, we will calculate the parameters of a single channel like in the ULA case.

At the beginning, the signal is captured by an antenna element of gain 2.15dBi and then, a circulator isolates the received from the transmitted signal. After that, an LNA of 15dB amplifies the signal since it is very weak and a BPF cuts off the out-of-band frequencies. So, the amplified signal enters the AIC block where a 8-bit phase shifter PS-255-2G18G-8B-SFF introduces a random phase shift. At the end, all the phase shifted signals are summed by an adder. The gain and the noise

figure of the phase shifter will be -3.5db and 11dB respectively [45]. The rest of the values of the parameters are drawn from an extensive analysis [46]. So, by adding these values to "RF Budget Analyzer" application [41], as shown in Figure 5-3, all the parameters of the channel are computed.

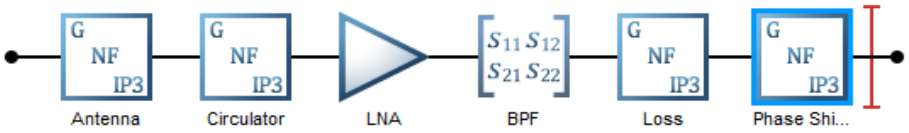

Stage	1	2	3	4	5	6
GainA (dB)	2.15	-1	15	-6.5e-13	-0.001	-3.5
NF (dB)	0	1	3.5	6.5e-13	0.01	11
OIP3 (dBm)	Inf	37	Inf	Inf	Inf	14.5

Cascade	1	1..2	1..3	1..4	1..5	1..6
Fout (GHz)	5.8	5.8	5.8	5.8	5.8	5.8
Pout (dBm)	-77.85	-78.85	-63.85	-63.85	-63.85	-67.35
GainT (dB)	2.15	1.15	16.15	16.15	16.15	12.65
NF (dB)	0	0.6364	3.239	3.239	3.24	3.783
OIP3 (dBm)	Inf	37	52	52	52	14.5
SNR (dB)	17.95	17.32	14.72	14.72	14.71	14.17

Figure 5-3: Calculated parameters of the first stage of AIC.

The next stage, consists of the superheterodyne receiver with the parameters calculated in Figure 5-2. As a result, we only have to put the values obtained in Figures 5-2, 5-3 in a row with an adder between them. A typical value for the gain for the adder is 1dB and a noise figure 1.56dB for device temperature equal to 125^oC [47]. Also, we will use $M = 100$ antenna elements in the ULA, which are reduced to $P = 50$ outputs. Consequently, we have the final calculation of the parameters of one channel of the AIC are indicated in Figure 5-4.

5-1-3 Comparison Between the Parameters of the Architectures

Before the comparison of the important parameters, we must also say some words about the other two architectures, the MC sampling and the ULMA. At first, in MC sampling, the number of channels is less than in ULA case. The same holds for the other two front-end schemes since in AIC there are M antenna elements and P outputs, and the number of outputs in ULMA is equal to the one in MC. So, in order to perform a fair comparison between their parameters, we must focus on the parameters per channel. Secondly, the channels in ULA and MC sampling are identical so we will consider that their parameters are the same per channel. Lastly, the channels in ULMA are identical to the ones in ULA and MC but the difference lies in the reception of the incident wave.

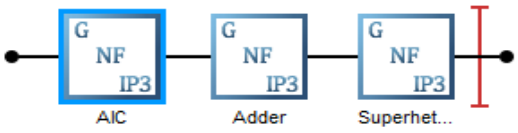

Stage	1	2	3
GainA (dB)	12.65	1	70.42
NF (dB)	3.783	1.56	3.974
OIP3 (dBm)	14.5	Inf	18.39

Cascade	1	1..2	1..3
Fout (GHz)	5.8	5.8	5.8
Pout (dBm)	-67.35	-66.35	4.07
GainT (dB)	12.65	13.65	84.07
NF (dB)	3.783	3.825	3.94
OIP3 (dBm)	14.5	15.5	18.39
SNR (dB)	14.17	14.13	14.01

Figure 5-4: Calculated parameters of one channel in AIC.

The results of the comparison are indicated in Figure 5-5 where we have the cascaded gain (Figure 5-5a), the cascaded SNR (Figure 5-5b), the noise figure (Figure 5-5c) and the IP3 (Figure 5-5d) of the signal at each stage in ULA, MC, AIC and ULMA architecture. At first, it is obvious that the number of components are different since in ULA case there are 15 components whereas in AIC, 17. Consequently, the complexity and the power consumption in AIC will be higher since there will be additive electronic and hardware adjustments between the components.

Concerning the important parameters, in Figure 5-5a, at each stage of the receiver we have a power gain which may increase or decrease depending on the respective component. For example, if the component is active, it increases the gain of the signal otherwise, passive components decrease the overall gain. In addition, we can see that the value of the overall gain introduced by ULA and MC sampling architecture to the signal is 86.57dB. On the other hand, in AIC case, the overall gain is 2dB lower i.e. 84.07dB. In the case of the ULMA of the same size, we may expect that the gain introduced by the metamaterial surface will be equal to the one of ULA. As a result, in our test case where the signal at the reception is really weak (-80dB), the signal power at the output will be 6.57dB in ULA, MC and ULMA whereas, it AIC will be 4.07dB.

On the other hand, the overall noise figure, shown in Figure 5-5c, depends mainly on the noise figure of the first components whereas the next stages have small effect on the overall noise figure so that it will have negligible variations, which is something that we expected from equation (2-13). For that reason, the total noise figure of the AIC is higher than the others due to the LNAs and the phase shifters placed at the beginning of the chain. Consequently, the SNR, shown in Figure

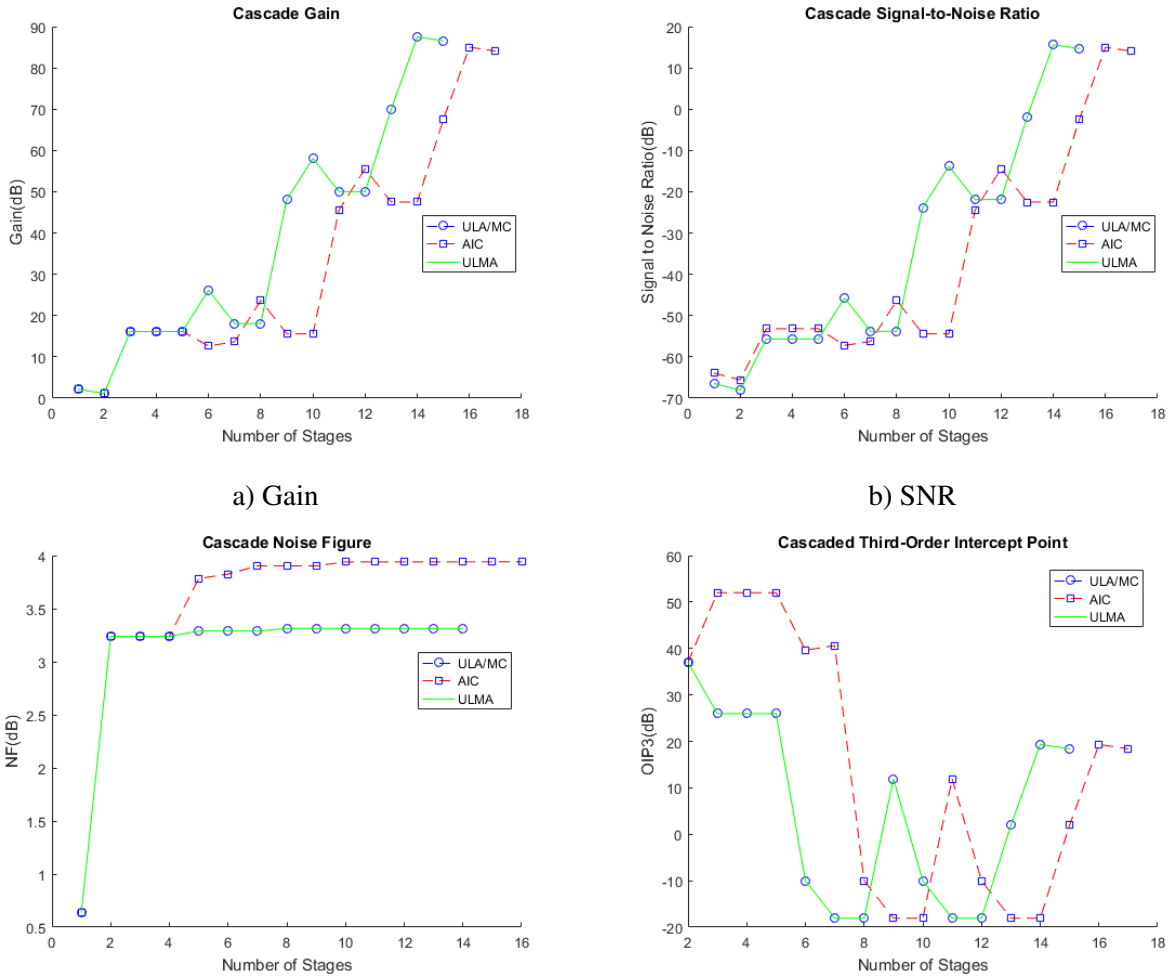

a) Gain

b) SNR

c) Noise figure

d) Third Order Intercept Point

Figure 5-5: Comparison between the parameters of ULA, MC, AIC and ULMA.

5-5b, will by higher in ULA case due to less thermal noise. Lastly, the output IP3 is the same for all the architectures despite the variations in the middle components.

5-2 Sparse Signal Processing

In this section, numerical results on DOA estimation illustrate each architecture. Moreover, we will demonstrate SSP in the back end while focusing on the compression matrix of each CS architecture. Lastly, the mutual coherence will be used as an extra performance metric.

Simulated data are used to demonstrate performance of SSP in the reference case ULA, in MC Sampling, AIC and ULMA. To keep the test simple and clear, we assume that there is only one target. We assume that the target is placed at 30^o. Also, we are sampling in space so the data that we will use, are referring to one time instant. In plain words, we will use only one snapshot and the measurements will have the form of equation 3-8. In ULA and AIC, the number of antenna elements will be $M = 100$ whereas, in MC it will be $P = 50$. In ULMA case, we will use a sigle metamaterial surface with 50 outputs. The main difference in the CS architectures lies in the number of outputs where in ULA is 100 and in all the rest is 50. That is because of the compression ration which we choose to be 0.5. The sensing matrix $\mathbf{\Psi}$ of each compressive sensing front end will contain the array vector responses of the angles in the estimation grid $-90 : 90$ with step $sin^{-1}(\frac{1}{M})$.

In order to formulate the measurements, the amplitude of each signal, the noise power and the SNRs per channel are drawn from equations calculated in the previous chapter. As a result, we can perform SSP in the three CS architectures using equations 4-14, 4-30, 4-40 and 4-46 and have matched filtering as a reference case. Figures 5-6a to 5-6e demonstrate the DOA estimation from SSP performed in yall1 [48]. In order to be more accurate, we perform 1000 iterations generating different random phase shifts and noise realizations each time in each case, and then we use the mean value to illustrate the SSP result. In that way, we eliminate the possibility of good or bad performance due to extreme values of random phase shifts.

As we can see, the results are satisfactory since the DOA estimation has been performed well. The SSP produces outcomes which are comparable to the ones in MF. So, since it is model-based, it can deconvolve MF with detection included. The magnitude of the reconstructed signal reflect the output power of the signal and the SNR and that is because SSP is searching for the signal which satisfies equation 3-9. For example, ULA has the highest performance along with ULMA. On the other hand, MC and has lower amplitude in the signal reconstruction due to the reduced number of antenna elements and AIC has the same amplitude as MC but with less output SNR because of the additional thermal noise, respectively.

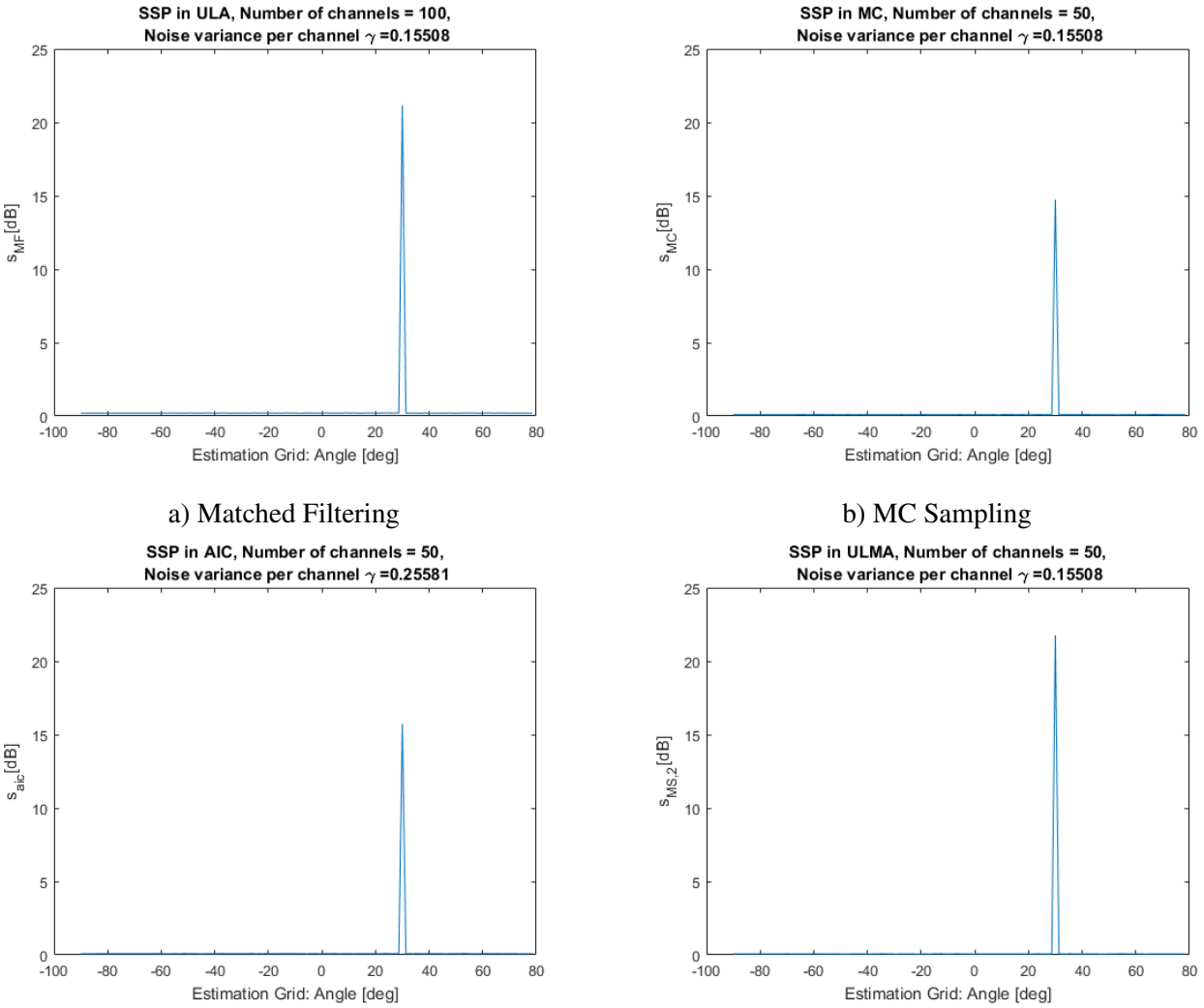

a) Matched Filtering

b) MC Sampling

c) AIC

d) ULMA

Figure 5-6: SSP in CS architectures.

Lastly, the mutual coherence $\mu(\boldsymbol{\Theta})$ given in equation 3-4 is taken into account and is plotted in Figure 5-7. As we have already mentioned, we are concerned with low coherence sensing matrices. So, the smaller the mutual coherence of $\boldsymbol{\Theta}$ is, the better the SSP performance (and the larger possible data compression) will be because, as we have said, an underdetermined system can be solved with SSP due to the sparsity of the signal and the incoherence of the sensing matrix. As we expected, the lowest mutual coherence is the one of the MF and that is because of the complete orthogonality of the square matched filtering matrix representing the estimation grid. The second lowest value of mutual coherence is the one of MC sampling with value 0.2393 due to the channel selection matrix H_{MC}. In fact, the system becomes underdetermined and the sensing matrix becomes less orthogonal. The mutual coherence of AIC is even higher and is almost the same as the one of ULMA which is something that we expected since they both have the same size of sensing matrix which is a full matrix, so it is the best mutual coherence we can get with the numbers of elements and output channels we assumed. This gives us the ability to state that we can have a novel architecture similar to the state-of-the-art AIC, with the same performance and mutual coherence, but without the use of phase shifters and additional amplifiers and intuitively, lower power consumption, additional costs and complexity.

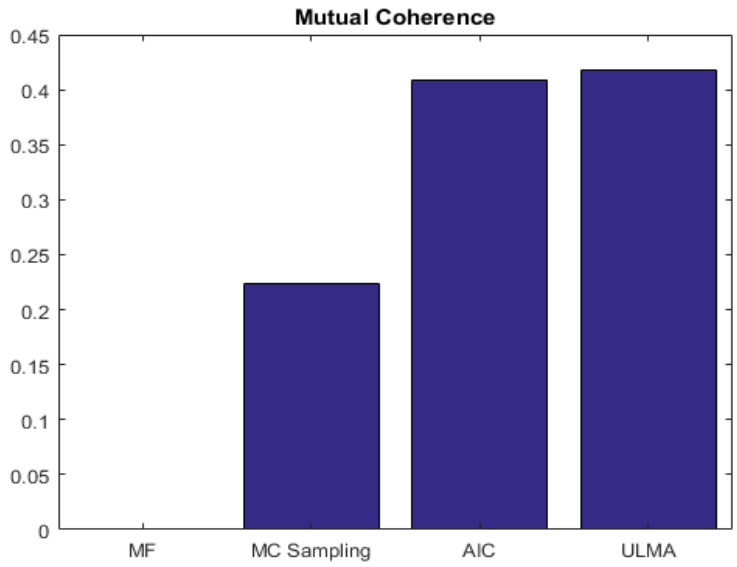

Figure 5-7: Mutual Coherence of each CS architecture.

Detailed Table				
Characteristics	ULA	MC	AIC	ULMA
# Input channels	M=100	P=50	M=100	M = 100
# Ouput channels	M=100	P=50	P=50	P=50
# Components	Mx15=1500	Px15=750	Mx6 + Px12 = 1150	Px15 = 750
Output Signal Power per channel[dB]	6.57	6.57	4.07	6.57
Output Noise Power per channel[dB]	-8.0944	-8.0944	-5.9294	-8.0944
Mean of the maximum total output SNR[dB]	34.6887	31.7322	29.9089	34.7371
Mutual Coh.	0	0.2393	0.4084	0.4177

Table 5-2: Detailed Characteristics of each CS architecture.

5-3 Performance - Complexity Analysis

For the performance-complexity analysis, all the details of each CS architecture are placed in a table where the differences of each architecture can be more obvious.

As we can see in Table 5-2, each radar front-end design that we have presented, have both advantages and disadvantages, depending on the perspective that they will be commented. At first, the ULA, AIC and the ULMA use the full aperture, i.e. have all M inputs, so they are using M antenna elements, twice more than in MC. In order to be able to refer to the cost in each architecture, we must count the number of all the components. In ULA, MC and ULMA, the total number of components equals the number of channels multiplied by the number of components at each channel, which is 15 as shown in Figure 5-1. On the other hand, in AIC, we count $MxP_1 + PxP_2$, where P_1 is the number of components in the first stage shown in Figure 5-3, and P_2 is the number of components of the superheterodyne receiver which is 10+1 as shown in Figure 5-2, plus the adder. All in all, we compute that the number of components in each architecture for M=100 and P=50 are 1500 for ULA, 750 for MC and ULMA and 1150 for the AIC. This gives us the ability to say that AIC, has the

higher complexity of all the CS radar front-end schemes with respect to the number of components. Intuitively, this also implies that AIC will have the highest power consumption, size and it will be the most expensive, as well.

Despite the fact that MC and ULMA have the lowest number of components, ULMA has an additional complexity factor in the antenna. Regarding the complexity in the hardware per channel, ULA and MC are equal. In AIC, as we have already mentioned, a lot of work must be done for the adjustment of the components so the complexity will be higher. In ULMA though, metamaterial surface antenna elements are used with dimensions and characteristics that need precise printed circuit board (PCB) design, manufacturing with possibly expensive equipment which may increase the respective complexity and the cost of the architecture. At first, we can see that ULA, MC and ULMA have the higher output gain and that is because they capture more signal power per output channel whereas the AIC has the lowest gain. We have also included the output noise power per channel where it is obvious that all the architectures produce the same noise power except AIC since it is the one with additional thermal noise.

Lastly, in Table 5-2 the mean value of the maximum output SNR per architecture after 1000 realizations, drawn from equations 4-23, 4-34, 4-45 and 4-50, indicates that ULA along with ULMA have the highest maximum output SNR since they capture more signal energy per output channel. In reality, ULMA might give a bit less SNR since the exact metasurface scattering is unknown and might cause SNR loss. This is something significant since we can say that we can obtain comparable performance to the reference case, but by using less outputs and metamaterial surfaces. On the other hand, MC sampling has 3dB less output SNR which is something that we expected since it uses half of the antennas of ULA and AIC has the lowest output SNR due to the highest output noise power.

Chapter 6

Conclusions and Future Work

In this chapter, we draw the final conclusions and suggest future steps that can be made as an extension of this research.

6-1 Conclusions

In this thesis, we studied several state-of-the-art radar receivers which are mainly used in modern radar systems. Our purpose is to focus on the front end with the implementation of compressive sensing. The main goal of this thesis is to present three CS front ends and evaluate them with respect to complexity and performance.

In the main body of the thesis, we analyzed four different radar front ends. The first one, is the conventional ULA where we have a number of equally spaced antenna elements which capture the received signal from the target signal. At first, we modeled the signal according to the narrowband approximation and specified all the details concerning the dimensions of the array and the power of the signal. Then, we presented two CS front-end radar architectures, the MC Sampling and the AIC where we get less data taking advantage of the sparsity of the signal. We formulated their sensing matrices and the SSP model which was used at the end. Lastly, we proposed a novel CS radar front-end architecture which consists of metamaterial surface antennas. These antennas, have the advantage

of scattering the incoming signal without the use of any additional hardware. In that way, we obtained less channels without additional thermal noise.

The main goal of the thesis is to present the balance between the performance and the complexity of each architecture. We saw that each CS front end has both advantages and disadvantages. At first, in the reference case of ULA the performance of the receiver is best since it introduces the highest SNR as shown in Figure 5-5b. The need of implementing CS arises in the size and the cost of the architecture since, as shown in Table 5-2, it needs the highest number of components and also, it is memory intensive since it uses the largest number of data. That is the purpose of implementing CS. In the next two state-of-the-art CS front ends, things are a bit more complicated. At first, we saw MC sampling which selects some of the channels of the ULA. In our case, we have chosen a compression ratio of 0.5 so the number of channels and components are halved. We have also computed the mutual coherence of the sensing matrix which has a low value and ensures the performance of the SSP.

In contrast to those two, AIC is an architecture which uses again less channels and less memory but it comes with additional costs. As we saw in the previous section, it contains more components than in MC so the power consumption and the overall size of the front end will be larger. In addition, the mutual coherence of its sensing matrix is higher. As a result, we understand that both performance and complexity are high. At the end, we introduced a novel CS radar front-end architecture which is using metamaterial surface antennas called ULMA. Its function is similar to the one of the AIC but with compressing the signal only at reception (with no receiver noise yet). Its main advantage is that it does that without the use of additional components like phase shifters, amplifiers and full adders.

In ULMA, despite the fact that mutual coherence is much higher than in the reference case, it shows comparable performance according to the output SNR. As a result, we have an architecture with very satisfying performance and less complexity, size, costs and memory usage. The exact nature of the metasurface scattering has been unknown, and may cause SNR loss.

Finally, the SNR loss in the favorite CS front-end architectures MC and ULMA could be compensated by better performance of the SSP in the back end. Thus, with CS applied in front and back end, comparable (if not better) performance and lower front-end complexity can be expected.

6-2 Future Work

- **Extension of the CS architecture in time domain.**

  In this thesis, we studied the CS only in spatial domain using one snapshot for each array of antenna elements. In that way, we were able to estimate only the angle of arrival of the target's signal. By sampling in both space and time domain, we could use methods to estimate range and velocity of the target.

- **Evaluation of the SSP performance**

  The main purpose of this thesis is to describe the balance between the performance and complexity in three CS front-end architectures. For that reason we analyzed the components of each architecture, and compared the respective important parameters. Though, for a complete characterization of the CS radar as a whole system, we need an evaluation of the SSP performance with respect to detection, accuracy and resolution. Accordingly, the case where targets are not positioned in the center of a cell in a discretized domain but anywhere (as in realistic cases) off the discrete grid would be relevant when evaluating the SSP performance.

- **Extension to multiple targets.**

  Our research focused only on DOA estimation of one target. But, this is not the case in general. In the case of having multiple targets, closely spaced, it would be relevant to investigate the resolution bounds [49].

- **Application of empty cavities in CS radar systems.**

  As we have mentioned in Section 4-5, an alternative way for capturing the signal could be to use empty cavities instead of metamaterial surface antennas. These cavities have the same behavior of the ULMA. The problem we have to deal with in that case, is that we must place a number of sensors inside these cavities in order to capture the signal. The spots in which the sensors are placed on, play an important role since they affect the sensing matrix which has to be as incoherent as possible.

- **Application of the ULMA architecture using frequency diversity.**

  As we mentioned in Section 4-5, the main advantage of the metamaterial surface antenna elements is the high diversity it introduces in both transmitting and receiving a backscattered field in different frequencies. For that reason, it can substitute AIC because of the less components.

So, in the case of using a radar which transmits linear frequency modulated pulses, despite the fact that the bandwidth of these pulses is rather small w.r.t. the carrier, the advantage of metamaterial surfaces would contribute to the incoherence of the sensing matrix.

Bibliography

[1] J. S. Richards, M. A. and W. A. Holm, *Principles of Modern Radar, Volume 1, Basic Principles*. Raleigh, NC: SciTech Pub., 2010.

[2] Skolnik and M. Ivan, *Radar handbook*. 1970.

[3] M. Loy, "Understanding and Enhancing Sensitivity in Receivers for Wireless Applications," *Wireless Communication Business Unit, TEXAS Instruments*, 1999.

[4] J. Crols and M. Steyaert, *CMOS Wireless Transceiver Design*. The Springer International Series in Engineering and Computer Science, Vol. 411, 1997.

[5] J. Tsui, *Digital Techniques for Wideband Receivers*. Artech House, Inc., 1995.

[6] S. Mallat, *A Wavelet Tour of Signal Processing: The Sparse Way*. Elsevier Inc., 2009.

[7] E. J. Candès and M. B. Wakin, "An Introduction to Compressive Sampling," *IEEE signal processing magazine 25.2: 21-30*, 2008.

[8] J. R. Candès, Emmanuel J. and T. Tao, "Robust Uncertainty Principles: Exact Signal Reconstruction from Highly Incomplete Frequency Information.," *IEEE Transactions on information theory 52.2 : 489-509*, 2006.

[9] D. L. Donoho, "Compressed Sensing," *IEEE Transactions on information theory 52.4 : 1289-1306*, 2006.

[10] L. Zegov, R. Pribić, and G. Leus, "Optimal Waveforms for Compressive Sensing Radar," *21st European Signal Processing Conference (EUSIPCO)*, 2013.

[11] R. Holger, "Compressive Sensing and Structured Random Matrices," *Theoretical Foundations and Numerical Methods for Sparse Recovery, 9, pp.1-92*, 2010.

[12] R. Pribić and I. Kyriakides, "Design of Sparse-signal Processing in Radar Systems," *IEEE International Conference on Acoustics, Speech and Signal Processing (ICASSP), Florence, pp. 5008-5011*, 2014.

[13] J. Fuchs, "The Generalized Likelihood Ratio Test and the Sparse Representations Approach," *vol. 6134, pp. 245–253, of ICISP in Lecture Notes in Computer Science. Springer Berlin Heidelberg*, 2010.

[14] V. Trees, *Optimum Array Processing, pt. IV of Detection Estimation and Modulation Theory*. John Wiley & Sons, Inc, 2002.

[15] D.-S. Yoo, "A Low Complexity Subspace-based DOA Estimation Algorithm with Uniform Linear Array Correlation Matrix Subsampling," *International Journal of Antennas and Propagation*, 2015.

[16] A. J. van der Veen and G. Leus, *Signal Processing for Communications*. Delft University of Technology, 2005.

[17] M. Mishali and Y. C. Eldar, "From Theory to Practice: Sub-Nyquist Sampling of Sparse Wideband Analog Signals," *IEEE Journal of Selected Topics in Signal Processing 4.2: 375-391*, 2010.

[18] M. Moshe, Y. C. Eldar, and A. J. Elron, "Xampling: Signal Acquisition and Processing in Union of Subspaces," *EEE Transactions on Signal Processing 59.10: 4719-4734*, 2011.

[19] P. Feng and Y. Bresler, "Spectrum-Blind Minimum-rate Sampling and Reconstruction of Multiband signals," *Acoustics, Speech, and Signal Processing, 1996. ICASSP-96. Conference Proceedings., 1996 IEEE International Conference on. Vol. 3. IEEE*, 1996.

[20] Y. Kochman and G. W. Wornell, "Finite Multi-coset Sampling and Sparse Arrays," *Information Theory and Applications Workshop (ITA). IEEE*, 2011.

[21] J. N. Laska, S. Kirolos, M. F. Duarte, T. S. Ragheb, R. G. Baraniuk, and Y. Massoud, "Theory and Implementation of an Analog-to-Information Converter using Random Demodulation," *Circuits and Systems, 2007. ISCAS*, 2007.

[22] S. Kirolos, J. Laska, M. Wakin, M. Duarte, D. Baron, T. Ragheb, Y. Massoud, and R. Baraniuk, "Analog-to-Information Conversion via Random Demodulation," *Design, Applications, Integration and Software, IEEE Dallas/CAS*, 2006.

[23] M. Wakin, S. Becker, E. Nakamura, M. Grant, E. Sovero, D. Ching, J. Yoo, J. Romberg, A. Emami-Neyestanak, and E. Candes, "A non-Uniform Sampler for Wideband Spectrally-Sparse Environments," *IEEE Journal on Emerging and Selected Topics in Circuits and Systems 2.3: 516-529*, 2012.

[24] S. M. Kay, *Fundamentals of Statistical Signal Processing. Vol I: Estimation Theory*. Prentice Hall PTR, 1993.

[25] S. M. Kay, *Fundamentals of Statistical Signal Processing. Vol II: Detection Theory*. Prentice Hall PTR, 1998.

[26] M. Boyarsky, T. Sleasman, L. Pulido-Mancera, T. Fromenteze, A. Pedross-Engel, C. M. Watts, M. F. Imani, M. S. Reynolds, , and D. R. Smith, "Synthetic Aperture Radar with Dynamic Metasurface Antennas: A Conceptual Development," *JOSA A, 34(5), A22-A36.*, 2017.

[27] H. Sato, K. Sawaya, K. Mizuno, J. Uemura, M. Takeda, J. Takahashi, K. Yamada, K. Morichika, T. Hasegawa, H. Hirai, H. Niikura, T. Matsuzaki, S. Kato, and J. Nakada, "Passive Millimeter-wave Imaging for Security and Safety Applications," *Proc. SPIE. Vol. 7671.*, 2010.

[28] R. Appleby and R. N. Anderton, "Millimeter-wave and Submillimeter-wave Imaging for Security and Surveillance," *Proc. IEEE. Vol. 95, No. 8*, 2007.

[29] D. J. Brady, *Optical Imaging and Spectroscopy*. Wiley-OSA, 2009.

[30] A. Moreira, P. Prats-Iraola, M. Younis, G. Krieger, I. Hajnsek, and K. P. Papathanassiou, "A Tutorial on Synthetic Aperture Radar," *IEEE Geoscience and Remote Sensing Magazine, vol. 1, no. 1, pp. 6-43*, 2013.

[31] Hunt, John, T. Driscoll, A. Mrozack, G. Lipworth, M. Reynolds, D. Brady, and D. R. Smith, "Metamaterial Apertures for Computational Imaging," *Science 339, no. 6117: 310-313*, 2013.

[32] G. Lipworth, A. Mrozack, J. Hunt, D. L. Marks, T. Driscoll, D. Brady, and D. R. Smith, "Metamaterial Apertures for Coherent Computational Imaging on the Physical Layer," *J. Opt. Soc. Am. A 30, 1603-1612*, 2013.

[33] J. Hunt, J. Gollub, T. Driscoll, G. Lipworth, A. Mrozack, M. S. Reynolds, D. J. Brady, , and D. R. Smith, "Metamaterial Microwave Holographic Imaging System," *J. Opt. Soc. Am. A 31, 2109-2119*, 2014.

[34] T. Sleasman, M. Boyarsky, M. F. Imani, J. N. Gollub, and D. R. Smith, "Design Considerations for a Dynamic Metamaterial Aperture for Computational Imaging at Microwave Frequencies," *J. Opt. Soc. Am. B 33, 1098-1111*, 2016.

[35] C. M. Watts, A. Pedross-Engel, D. R. Smith, and M. S. Reynolds, "X-band SAR Imaging with a Liquid-Crystal-Based Dynamic Metasurface Antenna," *J. Opt. Soc. Am. B 34, 300-306*, 2017.

[36] G. Lipworth, A. Rose, O. Yurduseven, V. R. Gowda, M. F. Imani, H. Odabasi, P. Trofatter, J. Gollub, and D. R. Smith, "Comprehensive Simulation Platform for a Metamaterial Imaging System," *Appl. Opt. 54, 9343-9353*, 2015.

[37] L. Pulido-Mancera, T. Fromenteze, T. Sleasman, M. Boyarsky, M. F. Imani, M. Reynolds, and D. Smith, "Application of Range Migration Algorithms to Imaging with a Dynamic Metasurface Antenna," *J. Opt. Soc. Am. B 33, 2082-2092*, 2016.

[38] Fromenteze, Thomas, O. Yurduseven, M. F. Imani, J. Gollub, C. Decroze, D. Carsenat, and D. R. Smith, "Computational Imaging using a Mode-mixing Cavity at Microwave Frequencies," *Applied Physics Letters 106, no. 19: 194104*, 2015.

[39] T. Fromenteze, E. L. Kpré, D. Carsenat, C. Decroze, and T. Sakamoto, "Single-Shot Compressive MIMO Radar Imaging Using a Two-Port Passive Device," *IEEE Access, vol. 4, no. , pp. 1050-1060*, 2016.

[40] C. Tzotzadinis, "Performance and Complexity of Data Acquisition in Compressive-sensing Radar (Restricted Annex)," *Thales Group*, 2017.

[41] mathworks.com, "Superheterodyne Receiver Using RF Budget Analyzer App." https://nl.mathworks.com/help/rf/examples/superheterodyne-receiver-using-rf-budget-analyzer-app.html. Accessed: 01.09.2017.

[42] ETLSystems, "C-band Circulator Model: CIR01CXP-7514." http://www.etlsystems.com/products/1676-c-band-circulator-model-cir01cxp-7514. Accessed: 16.10.2017.

[43] C. Razzell, "System Noise-Figure Analysis for Modern Radio Receivers," *Maxim Integrated Tutorial 5594*, 2013.

[44] H. Zhou and B. Luo, "Design and Budget Analysis of RF Receiver of 5.8 GHz ETC reader," *Communication Technology (ICCT), 12th IEEE International Conference, Nanjing, China*, 2010.

[45] gtmicrowave.com, "Digital Phase Shifter P8P-39N-5JD." $http://www.gtmicrowave.com/digital_phase_shifter_p8p_39n_5jd.php$. Accessed: 24.10.2017.

[46] K. J. Koh and G. M. Rebeiz, "An X - and Ku - Band 8-Element Phased-Array Receiver in 0.18 - μm SiGe BiCMOS Technology," *IEEE Journal of Solid-State Circuits, vol. 43, no. 6, pp. 1360-1371*, 2008.

[47] Electronics-Tutorials.com, "Unity Gain Inverting Adder." http://www.electronics-tutorials.ws/opamp/opamp4.html. Accessed: 24.10.2017.

[48] yall1: your algorithms for L1. http://yall1.blogs.rice.edu/.

[49] R. Pribić and G. Leus, "Information Distances for Radar Resolution Analysis," *IEEE CAMSAP*, 2017.

